

# Systems Science & Control Engineering

An Open Access Journal

ISSN: (Print) (Online) Journal homepage: [www.tandfonline.com/journals/tssc20](http://www.tandfonline.com/journals/tssc20)

## Dual FOPID-neural network controller based on fast grey wolf optimizer: application to two-inputs two-outputs helicopter

Amar Rezoug, Jamshed Iqbal & Abdelkrim Nemra

To cite this article: Amar Rezoug, Jamshed Iqbal & Abdelkrim Nemra (2025) Dual FOPID-neural network controller based on fast grey wolf optimizer: application to two-inputs two-outputs helicopter, Systems Science & Control Engineering, 13:1, 2449156, DOI: [10.1080/21642583.2024.2449156](https://doi.org/10.1080/21642583.2024.2449156)

To link to this article: <https://doi.org/10.1080/21642583.2024.2449156>



© 2025 The Author(s). Published by Informa UK Limited, trading as Taylor & Francis Group.



Published online: 12 Jan 2025.



Submit your article to this journal [↗](#)



View related articles [↗](#)



View Crossmark data [↗](#)

# Dual FOPID-neural network controller based on fast grey wolf optimizer: application to two-inputs two-outputs helicopter

Amar Rezoug<sup>a</sup>, Jamshed Iqbal<sup>b</sup> and Abdelkrim Nemra<sup>c</sup>

<sup>a</sup>Laboratoire des Technologies Innovantes, Ecole Nationale Supérieure des Technologies Avancées, Diplomatic City, Dergana-Bordj El Kiffan, Algiers, Algeria; <sup>b</sup>School of Computer Science, Faculty of Science and Engineering, University of Hull, Hull, UK; <sup>c</sup>Laboratoire Guidage et Navigation, Ecole Militaire Polytechniques, Bordj El Bahri, Algiers, Algeria

## ABSTRACT

This research introduces a novel dual Fast Grey Wolf Optimizer (FGWO) combined with Radial Basis Function Neural Networks (RBFNN) for a Fractional-Order PID (FOPID) controller applied to a helicopter simulator. The proposed FGWO improves the standard Grey Wolf Optimizer (GWO) by enhancing hunting during the exploitation phase and increases robustness in convergence to the minimum value. FGWO optimizes the FOPID parameters using a novel objective function. The RBFNN is integrated to address the nonlinearities and uncertainties, while a dual block mitigates the coupling effects. The performance of the proposed controller is characterized by two simulation scenarios. The first scenario involved nine benchmark functions across thirty trials. Results demonstrated that the FGWO offered superior performance in terms of robustness and proximity to the global minimum compared to the GWO. The second scenario involved applying the controllers to the helicopter. Results evidenced that the dual-FOPID-FGWO (DRF-FG) controller achieved a 4.3363% faster response and 1.8199% higher precision than the GWO-based controller (DRF-G). The DRF-FG showed robustness in trajectory tracking compared to the controllers based on the Ant Lion Optimizer (DRF-A) and the Whale Optimization Algorithm (DRF-W). DRF-FG improved the average regulation performance by 1.702% and trajectory tracking by 0.152% compared with DRF-G.

## ARTICLE HISTORY

Received 15 July 2024  
Accepted 27 December 2024

## KEYWORDS

Metaheuristic optimization; fractional-order PID controller; fast grey wolf optimizer; helicopter control

## 1. Introduction

Unmanned Aerial Vehicles (UAVs) have been widely employed in military and civilian domains (Tutsoy et al., 2024). Numerous UAV configurations are currently operational, among these configurations, the traditional Two Inputs Two Outputs (TITO) Sikorsky helicopter is particularly useful, owing to its distinct features such as Vertical Take Off and Landing (VTOL) capability, compact tail design, and relatively modest power consumption with only two rotors. UAV simulators emulate laboratory equipment to facilitate the safe assessment of control algorithms. These systems enable researchers to closely replicate the dynamics of real UAVs while minimizing the cost associated with experimentation by reducing the risks associated with damages to the actual operational units. Scientific literature reports several examples of helicopter simulators such as Gopmandal and Ghosh (2022); Hoffman et al. (2018); Norsahperi and Danapalasingam (2020); Zhu and Li (2021).

TITO helicopter is a highly nonlinear and uncertain aerodynamic Multiple-input multiple-output (MIMO) system with cross-coupled dynamics. In addition, it should

be able to fly safely in a disturbed environment. In order to stabilize such a system, controllers based on linear and nonlinear methods have been investigated (Irfan et al., 2024). A nonlinear controller based on prescribed-time-constrained feedback approach was reported in Singh et al. (2023). Variants of integral backstepping control were proposed in Haruna et al. (2023); Haruna et al. (2020). A non-singular MIMO adaptive-optimal Terminal Sliding mode control approach was proposed in Rezoug et al. (2024). The aforementioned studies present complicated design approaches that pose challenges in their real-time control particularly on a physical UAV. On the other hand, Proportional Integral Derivative (PID) and its variants have also been proposed in recent years for controlling TITO helicopters. A few exemplary works include Faisal and Abdulwahhab (2021); Norsahperi and Danapalasingam (2020); Pathan et al. (2021); Shah et al. (2023); Shalaby et al. (2023); Żegleń-Włodarczyk (2023). However, for highly nonlinear systems, the use of PID control may not be the best-recommended choice because of its constrained ability to provide satisfactory performance and robustness in a small area around the setpoint

**CONTACT** Jamshed Iqbal  [j.iqbal@hull.ac.uk](mailto:j.iqbal@hull.ac.uk)

(Haq et al., 2022). In order to obtain the best performance with robustness, Fractional Order PID (FOPID) was proposed, in which the parameters must be tuned according to the system dynamics. The tuning of FOPID controllers has garnered significant attention from the control community, particularly regarding reducing the number of parameters required when dealing with complex systems (Iqbal et al., 2015). FOPID was applied to UAV systems, as reviewed in Lopez-Sanchez and Moreno-Valenzuela (2023). In Norsahperi and Danapalasingam (2020); Shalaby et al. (2023); Żegleń-Włodarczyk (2023), optimized FOPID controllers based on metaheuristic algorithms were successfully applied, where optimization determined the optimal values of the control parameters.

In addition to FOPID controllers, metaheuristic techniques have also been extensively considered over the last decade for other controllers (Izci & Ekinci, 2023; Izci et al., 2023; Karakoyun et al., 2020; Lv et al., 2022; Oliveira et al., 2020; Sun & Miao, 2023; Zatout et al., 2022; Zhang et al., 2022). The Grey Wolf Optimizer (GWO) is a relatively new metaheuristic algorithm proposed (Mirjalili et al., 2014). The GWO emulates the social hierarchy of wolves' leadership, which is well known for hunting in packs. GWO is relatively faster and simpler since it uses a minimal number of adjustable parameters. Its efficiency has been demonstrated in diverse fields through numerous applications (Makhadmeh et al., 2024; Mirjalili et al., 2014; Rezoug et al., 2022). Compared to other swarm intelligence algorithms, GWO requires fewer tuning parameters, which simplifies the optimization process. This is different from algorithms like Particle Swarm Optimization (PSO), WOA and ALO which rely on individual experiences. It is reported in Makhadmeh et al. (2024) that owing to its effective exploitation strategy, GWO often exhibits superior convergence properties, whereas other algorithms may require more iterations to converge. In addition, GWO uses a unique mathematical model to simulate the encircling and hunting behaviour of wolves, while other algorithms may utilize different strategies (e.g. PSO relies on velocity updates based on personal and group bests). Despite several advantages offered by GWO, it suffers from premature convergence to the minimum with a possibility of stagnation in the local minimum and abrupt transition from exploration to exploitation. In order to address these issues and improve the performance of classical approaches, variants of the GWO have been proposed in recent years. These variants can be subdivided into two main categories in terms of mode of improvement (Makhadmeh et al., 2024); (i) structural modification of GWO and (ii) hybridization of GWO with other algorithms. The objective of the first approach is to modify the structure by including terms in the exploration and/or exploitation phase (Huang et al., 2021; Karakoyun

et al., 2020; Luo, 2019; Yingxun et al., 2020). The second approach involves combining GWO with Artificial Intelligence (AI) based algorithms to address the inherent demerits of GWO by Jarray et al. (2022); Lv et al. (2022); Qu et al. (2020). In comparison to the first approach, the second method may pose challenges in terms of parameter adjustment and require an optimal balance between GWO and the AI method used.

Neural Networks (NN) is an active research topic in the scientific community. This method is useful when dealing with complex systems that are challenging to model and are therefore difficult to control. The conventional NN has fundamental problems of slow learning time and stagnation in local minima (Veerasingam et al., 2022). To address these problems, the concept of Radial Based Function Neural Networks (RBFNN) (Zijie et al., 2022) is proposed as an alternative of the multi-layers NN. The RBFNN has a single hidden layer and thus offers quick learning. The RBFNN is widely used to control nonlinear systems owing to its superior speed performance and can be used individually or in combination with other control methods. PID- and FOPID-based NN controllers have been proposed and applied to various systems (Veerasingam et al., 2022; Zijie et al., 2022). Relevant notable works on RBFNN include adaptive RBFNN for a robotic manipulator (Liu et al., 2021), adaptive PI and RBFNN PID for a permanent magnet synchronous motor (PMSM) drive (Zeng et al., 2022) and a quadrotor UAV (Guo et al., 2023). In these research works, it is clearly shown that the RBFNN offers superior performance compared to the conventional NN in many applications. The optimizations of RBFNN using the GWO algorithm have been investigated in several contexts including; (i) the parametric optimization of RBFNN by GWO (ii) the combination of RBFNN with another controller optimized by GWO and (iii) the adjustment of RBFNN output using GWO. For the first context, interested readers are referred to notable recent works using GWO such as; Wu et al. (2023) estimated parameters in a lithium-ion battery indicating its state of health, Hussein and Al-Araji (2024) found optimal parameters in a hovercraft indicating its optimal path, Wang et al. (2022) enhanced image reconstruction accuracy to improve the resolution of electrical impedance tomography imaging and Chen et al. (2022) predicted the undrained shear strength by examining cone penetration. An example of the second context is reported in Messaoui et al. (2024), where RBFNN has been used to adjust the PID-based GWO controller applied to a 3-DOF helicopter laboratory system. An example of the third context is presented in Sreedhar et al. (2024), where GWO has been employed to fine-tune output of RBFNN for the maximum power point tracking (MPPT) problem. GWO variants have been successfully used to solve control

problems, such as tuning the fuzzy logic controller to enhance the performance of a sun-tracker system (Tripathi et al., 2020). In Zhang and Ming (2021), the dynamic GWO has been proposed to optimize the Type-2 fuzzy logic control law. In Shauqee et al. (2021), hybridization of a proportional double derivative with a Linear Quadratic controller (PD2-LQR)-based improvised GWO controller was designed to control a quadrotor system. In Choubey and Ohri (2022), PID gain parameters based on GWO-LQR weighting matrices have been proposed. Other GWO variants have been applied to different systems, such as a serial robotic manipulator (Rezoug et al., 2022) and a 3-Degree Of Freedom (DOF) parallel manipulator (Choubey & Ohri, 2023). These new approaches provide relatively better results than classical GWO.

In the light of the aforementioned studies, some important aspects are not fully considered such as, in many works, FOPID controller has been applied as a Single-Input Single-Output (SISO) controller with the cross-coupling effect ignored. The use of MIMO-NN offers several challenges in terms of its structural adjustment. To the best of the authors knowledge, as of now, the optimization of FOPID by GWO in the context of TITO helicopter simulator has not been addressed. A few works addressed the dual control aspect for this class of system and thus it remained an active problem in the control community.

In this study, we propose a new optimized Dual-RBFNN-FOPID-FGWO (DRF-FG) controller that combines the simplicity and robustness of the FOPID and flexibility of the RBFNN thus improving the control performance and system stability. The FOPID parameters are tuned using an optimized procedure based on Fast GWO (FGWO). In addition, a dual approach is employed to mitigate the cross-coupling effect. The overall principle of this research can be summarized as follows: (1) control using a classical FOPID controller, (2) optimize FOPID parameters using FGWO, (3) adjust the FOPID parameters using RBFNN controller and (4) involve dual control to handle cross-coupling effect. The proposed DRF-FG addresses the since the control approach is both adaptive and optimal. The optimization is related to the FOPID parameters designed using FGWO and the adaptation is a consequence of incorporating the RBFNN into each FOPID action. The RBFNN is well known to handle nonlinearities and uncertainties in a system. Thus, knowledge of precise parameters of the system is not required to apply the proposed approach. The contributions of this study are summarized as follows:

- (i) Proposing a new metaheuristic approach based on the GWO. This approach, named as FGWO, improves hunting during the exploitation phase.

The proposed approach was validated using nine benchmark fitness functions.

- (ii) Using FGWO to design FOPID parameters with an application to the trajectory tracking of a TITO Quanser Aero helicopter.
- (iii) Proposing a new hybrid controller based on FGWO-FOPID discussed in (ii) and the integrated RBFNN. The RBFNN relies on online learning and thus eliminates the need of a training phase. The dual algorithm is incorporated into the proposed hybrid controller to deal with cross-coupling.
- (iv) The effectiveness of the DRF-FG scheme is confirmed through several simulations using the TITO Quanser Aero simulator and its performance was compared with those of Dual-RBFNN-FOPID-GWO (DRF-G), Dual-RBFNN-FOPID-ALO (DRF-A), and Dual-RBFNN-FOPID-WOA (DRF-W). The results demonstrated the superior performance of the proposed controller.

The remainder of the paper is organized as follows: Section 2 presents the background of GWO, FOPID, and RBFNN. In Section 3, the optimization of FOPID parameters using GWO and its variants is presented. The application of the proposed method and its comparison with classical and optimized FOPID are presented in Section 4. The design of Dual-RBFNN-FOPID-FGWO (DRF-FG) is discussed in Section 5. The simulation results are presented in Section 6. Finally, Section 7 concludes the paper.

## 2. The Quanser Aero helicopter description and modelling

The Quanser Aero system, shown in Figure 1, is a 2-degree-of-freedom (2DOF) system consisting of a base on which a vertical arm is mounted. The helicopter is attached to the top of this vertical axis. The helicopter itself is attached at the midpoint of this arm. The rotors are housed within protective casings with counterweights fixed at each casing. The system is equipped with incremental angle sensors, one for each axis, allowing for the measurement of angles and their velocities. The two rotors can be controlled independently. A main rotor and a tail rotor are positioned at either end of the beam (Choubey & Ohri, 2022). Both rotors are driven by DC motors (Zhu & Li, 2021) operating within a voltage range of  $\pm 24$  V. The helicopter is a rotary-wing aircraft whose propulsion is provided by rotors that allow manoeuvring to reach accessible places. The helicopter simulator is a prototype that allows angular movements in pitch and yaw axes. The system finds potential in the validation of control approaches with a relatively high degree of applicability to real helicopters. Given its physical similarity to

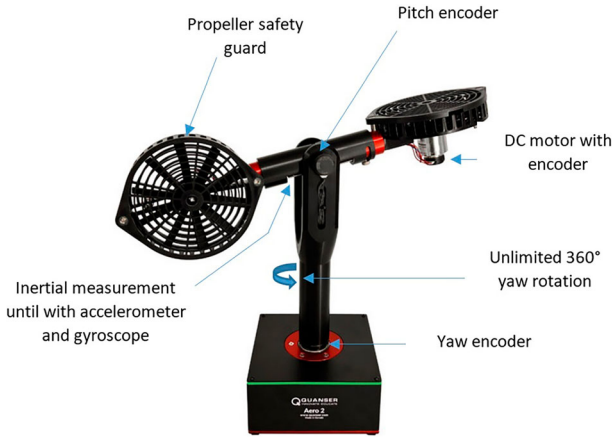


**Figure 1.** Quanser Aero system.

**Table 1.** Physical Aero Quanser parameters.

Description	Symbol	Value	Unit
Mass	$m$	1.075	kg
Pitch directional viscous damping	$D_p$	-7.59	N/V
Yaw directional viscous damping	$D_y$	15.8	N/V
Pitch inertia	$J_p$	$2.15 \times 10^{-2}$	kgm <sup>2</sup>
Yaw inertia	$J_y$	$2.37 \times 10^{-2}$	kgm <sup>2</sup>
Drag/air resistance coefficient	$k_d$	$1 \times 10^{-5}$	Nm
Acceleration due to gravity	$g$	9.81	ms <sup>-2</sup>
Input voltage of pitch angle	$V_p$		V
Input voltage of yaw angle	$V_y$		V
Distance between centre of mass and origin of B	$l_c$	0.002	mm
Torque thrust gain from the pitch rotor	$K_{pp}$	-	-
Cross-torque thrust gain exerted on the pitch from the yaw rotor	$K_{py}$	-	-
Cross-torque thrust gain applied on the yaw from the pitch rotor	$K_{yp}$	-	-
Torque thrust gain from the yaw rotor	$K_{yy}$	-	-

a real helicopter, the Quanser Aero has the same configuration as a helicopter i.e. the main propeller provides the system with the necessary power and tail propeller stabilizes the system. The system parameters are listed in Table 1.

The forces acting on the system are expressed in the fixed frame (Figure 1). The voltage  $V_p$  applied to the pitch motor generates a force  $F_p$  perpendicular to the body at a distance  $r_p$  from the pitch axis. Similarly, the yaw motor produces a force  $F_y$  due to the voltage  $V_y$ . This force acts at a distance  $r_y$  from the yaw axis and also induces a torque around the pitch axis. The rotation of the pitch rotor creates a torque around the motor, influencing the motion around the yaw axis. Consequently, the rotation of the pitch rotor causes movement around both the pitch axis and the yaw axis.

To develop the nonlinear model of the Quanser Aero, the following assumptions are considered: (i) Both rotors have identical dimensions and are positioned at equal distances from the centre of rotation, (ii) The pitch angle

is parallel to the ground, meaning the pitch is zero (iii) The pitch angle is positive when the front rotor moves upward, with a positive voltage applied to the front rotor (iv) The yaw angle is positive when the body rotates counterclockwise around the  $z$  axis, with a positive voltage applied to the tail rotor.

The centre of mass of the fixed body is expressed in Cartesian coordinates as

$$\begin{cases} x_c = l_c \cos \psi \cos \theta \\ y_c = l_c \sin \psi \cos \theta \\ z_c = l_c \sin \theta \end{cases} \quad (1)$$

where  $\theta$  and  $\psi$  are pitch angle and yaw angle respectively. In this system, there is only one potential energy  $E_{\text{pot}}$ , which arises from the gravitational force and is expressed as

$$E_{\text{pot}} = mgl_c \sin \theta \quad (2)$$

There are three kinetic energies associated with the system; the rotational kinetic energies on the pitch ( $E_{\text{kin}_1}$ ) and yaw axes ( $E_{\text{kin}_2}$ ) and the kinetic energy generated by the translational movement of the centre of mass ( $E_{\text{kin}_3}$ ). These energies are written as,

$$\begin{cases} E_{\text{kin}_1} = \frac{1}{2} J_p \dot{\theta}^2 \\ E_{\text{kin}_2} = \frac{1}{2} J_y \dot{\psi}^2 \\ E_{\text{kin}_3} = \frac{1}{2} ml_c^2 \begin{bmatrix} (-\sin(\psi) \cos(\theta) \dot{\psi} \\ -\cos(\psi) \sin(\theta) \dot{\theta})^2 \\ +(\sin(\psi) \sin(\theta) \dot{\theta} - \cos(\psi) \cos(\theta) \dot{\psi}) \\ +(\cos(\theta) \dot{\theta})^2 \end{bmatrix} \end{cases}$$

The total kinetic energy ( $E_{\text{kin}}$ ) of the system is the sum of  $E_{\text{kin}_1}$ ,  $E_{\text{kin}_2}$  and  $E_{\text{kin}_3}$  then

$$E_{\text{kin}} = E_{\text{kin}_1} + E_{\text{kin}_2} + E_{\text{kin}_3} \quad (3)$$

Putting the values of kinematic energies,

$$E_{\text{kin}} = \frac{1}{2} (J_p \dot{\theta}^2 + J_y \dot{\psi}^2 + ml_c^2 \dot{\psi}^2 \cos^2 \theta + ml_c^2 \dot{\theta}^2) \quad (4)$$

Lagrange's equation is used to find the equations of motion for the pitch and yaw as,

$$\left. \begin{aligned} \frac{\partial}{\partial t} \left( \frac{d\Lambda}{d\dot{\theta}} \right) - \frac{d\Lambda}{d\theta} &= F_p \\ \frac{\partial}{\partial t} \left( \frac{d\Lambda}{d\dot{\psi}} \right) - \frac{d\Lambda}{d\psi} &= F_y \end{aligned} \right\} \quad (5)$$

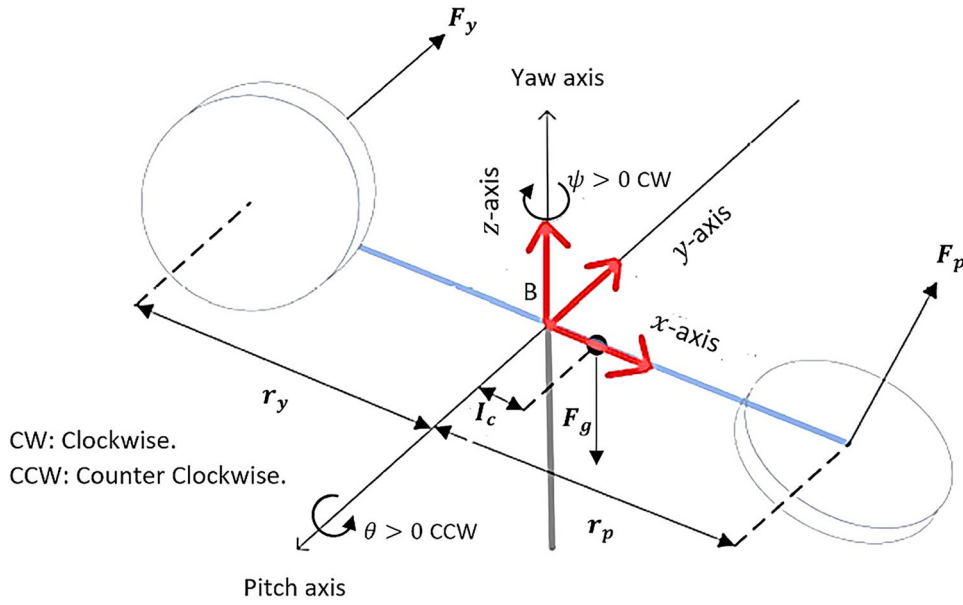


**Figure 2.** Frame assignment on Quanser Aero system.

where  $\Lambda$  is the Lagrangian operator.  $F_p$  and  $F_y$  are the forces applied along the pitch axis and the yaw axis respectively.

$$\begin{cases} F_p = \tau_{\text{pitch}} - D_p \dot{\theta} \\ F_y = \tau_{\text{yaw}} - D_y \dot{\psi} \end{cases} \quad (6)$$

where

$$\begin{cases} \tau_{\text{pitch}} = K_{pp} V_p + K_{py} V_y \\ \tau_{\text{yaw}} = K_{yp} V_p + K_{yy} V_y \end{cases} \quad (7)$$

where  $\tau_{\text{pitch}}$  and  $\tau_{\text{yaw}}$  are the torques produced by the pitch and yaw motors respectively.  $K_{yy}$ ,  $K_{yp}$ ,  $K_{py}$  and  $K_{pp}$ , respectively, represent the torque thrust gain from the yaw rotor, the cross-torque thrust gain affecting the yaw from the pitch rotor, the cross-torque thrust gain affecting the pitch from the yaw rotor and the torque thrust gain from the pitch rotor. Utilizing the Lagrange formulation (5) and considering the frames and forces applied to the system (shown in Figure 2) and given in (1–7), the dynamics of the Quanser Aero system helicopter is expressed as (Rezoug et al., 2024),

$$\begin{cases} (J_p + ml_c^2) \ddot{\theta} = (K_{pp} V_p + K_{py} V_y - D_p \dot{\theta} - mgl_c \cos(\theta) - ml_c^2 \dot{\psi}^2 \sin(\theta) \cos(\theta)) \\ (J_y + ml_c^2 \cos^2(\theta)) \ddot{\psi} = (K_{yp} V_p + K_{yy} V_y - D_y \dot{\psi} + 2ml_c^2 \dot{\theta} \dot{\psi} \sin(\theta) \cos(\theta)) \end{cases} \quad (8)$$

The model given in (8) indicates that the Quanser Aero system helicopter is a nonlinear and multivariable system with coupled dynamics.

Given a reasonably small value of  $l_c$  (see Table 1), we can consider the terms involving  $l_c^2$  to be negligible. The following remark is given:

**Remark 2.1:** If we to compare the first term of (8) (i.e.  $J_p + ml_c^2$ ), we have  $ml_c^2 = 1.075 \times (0.002 \times 0.01)^2 = 4 \times 10^{-12}$ , which is negligible compared to  $J_p = 2.15 \times 10^{-2}$ . The same observation can be made in the case of  $(J_y + ml_c^2 \cos^2(\theta))$ , since  $0 < \cos^2(\theta) < 1$ , thus,  $ml_c^2$  is negligible compared to  $J_y$ . For terms  $ml_c^2 \dot{\psi}^2 \sin(\theta) \cos(\theta)$  and  $2ml_c^2 \dot{\theta} \dot{\psi} \sin(\theta) \cos(\theta)$ , since  $|\sin(\theta) \cos(\theta)| < 1$  and the velocities of the two motors are limited,  $l_c^2$  make these terms negligible.

Therefore, (8) can be rewritten as

$$\begin{cases} J_p \ddot{\theta} = (K_{pp} V_p + K_{py} V_y - D_p \dot{\theta} - mgl_c \cos(\theta)) \\ J_y \ddot{\psi} = (K_{yp} V_p + K_{yy} V_y - D_y \dot{\psi}) \end{cases} \quad (9)$$

Assuming  $\cos(\theta) \approx \theta$ , the model given in (9) can be written as a linear MIMO system (10),

$$\begin{cases} J_p \ddot{\theta} = (K_{pp} V_p + K_{py} V_y - D_p \dot{\theta} - mgl_c \theta) \\ J_y \ddot{\psi} = (K_{yp} V_p + K_{yy} V_y - D_y \dot{\psi}) \end{cases} \quad (10)$$

Equation (10) represents a linear MIMO system with cross-coupled dynamics as shown in Figure 3, Similar model is given in Aero 2 (2024) and a more simplified version is reported in Dandago et al. (2024). Because the Quanser Aero is a coupled system, both control inputs are applied in the pitch and yaw angles, i.e.

$$\begin{cases} \theta = \theta_{V_p} + \theta_{V_y} \\ \psi = \psi_{V_y} + \psi_{V_p} \end{cases} \quad (11)$$

where  $\theta_{V_p}$  and  $\psi_{V_y}$  are the output angles resulting from the principal control inputs,  $\theta_{V_y}$  and  $\psi_{V_p}$  are the angles representing the dynamic coupling and are associated with yaw loop control and pitch loop control respectively.

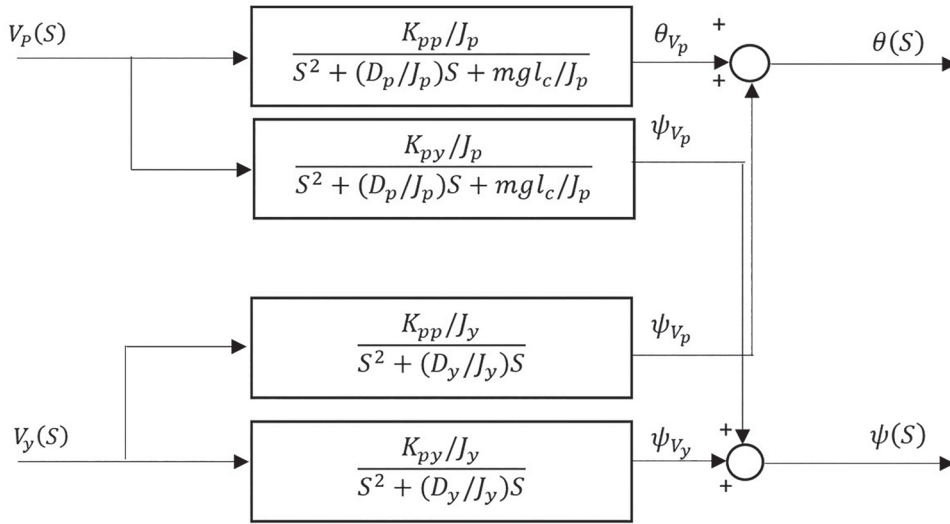


**Figure 3.** Dynamic model of TITO helicopter.

The transfer function matrix of the Quanser Aero system can be written as

$$\begin{bmatrix} \theta(S) \\ \psi(S) \end{bmatrix} = \begin{bmatrix} \frac{K_{pp}/J_p}{S^2 + (D_p/J_p)S + mgl_c/J_p} & \frac{K_{py}/J_p}{S^2 + (D_p/J_p)S + mgl_c/J_p} \\ \frac{K_{pp}/J_y}{S^2 + (D_y/J_y)S} & \frac{K_{py}/J_y}{S^2 + (D_y/J_y)S} \end{bmatrix} \times \begin{bmatrix} V_p(S) \\ V_y(S) \end{bmatrix} \quad (12)$$

**Remark 2.2:** The nonlinear part in (8) can be considered as the uncertainties of the system, which will be handled by the controller.

### 3. Control design

In this section, the FOPID, dual-boundary law and RBFNN are presented. In addition, the theoretical backgrounds of GWO, FOPID, and RBFNN theories are summarized.

#### 3.1. PID and FOPID controllers

PID controller uses three terms to manipulate the error signal ( $e$ ). The error is the difference between the desired signal ( $y_d$ ) and the actual signal ( $y$ ). PID control law, in time and frequency domains, can be respectively

written as,

$$\left. \begin{aligned} u(t) &= K_p e(t) + K_I \int_{t_0}^{t_f} e(t) dt + K_D \frac{de(t)}{dt} \\ U(S) &= \left( K_p + K_I \frac{1}{S} + K_D S \right) E(S) \end{aligned} \right\} \quad (13)$$

where  $K_p$  is the proportional gain to scale the current error,  $K_I$  is the integral gain associated with the sum of previous errors and  $K_D$  is the derivative gain relevant to the rate of changes in the error signal.

The FOPID is a generalization of the classical PID and was proposed by Podlubny with the transfer function given in (14) (Lopez-Sanchez & Moreno-Valenzuela, 2023)

$$\left. \begin{aligned} u(t) &= K_p e(t) + K_I \int_{t_0}^{t_f} e(t) dt^\lambda + K_D \frac{d^\mu e(t)}{dt^\mu} \\ U(S) &= \left( K_p + \frac{K_I}{S^\lambda} + K_D S^\mu \right) E(S) \end{aligned} \right\} \quad (14)$$

where  $K_p$ ,  $K_I$  and  $K_D$  are real numbers and  $0 < \lambda < 1$  and  $0 < \mu < 1$  are positive real numbers. With  $\lambda = \mu = 1$ , the FOPID becomes the classical PID controller. FOPID scheme is shown in Figure 4.

#### 3.2. Dual-boundary law

Quanser Aero system is a TITO system and thus suffers from cross-coupling; the first input affects the second output (yaw output) and similarly, the second input affects the first input (pitch output). In the trajectory tracking mode, cross-coupling can lead to a state-space error. To

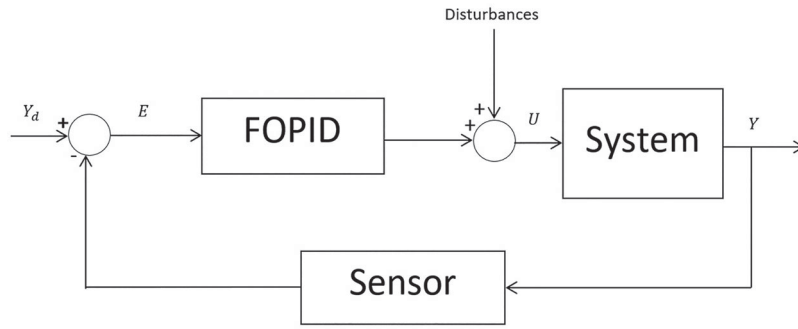


**Figure 4.** Overall closed-loop system containing FOPID controller.

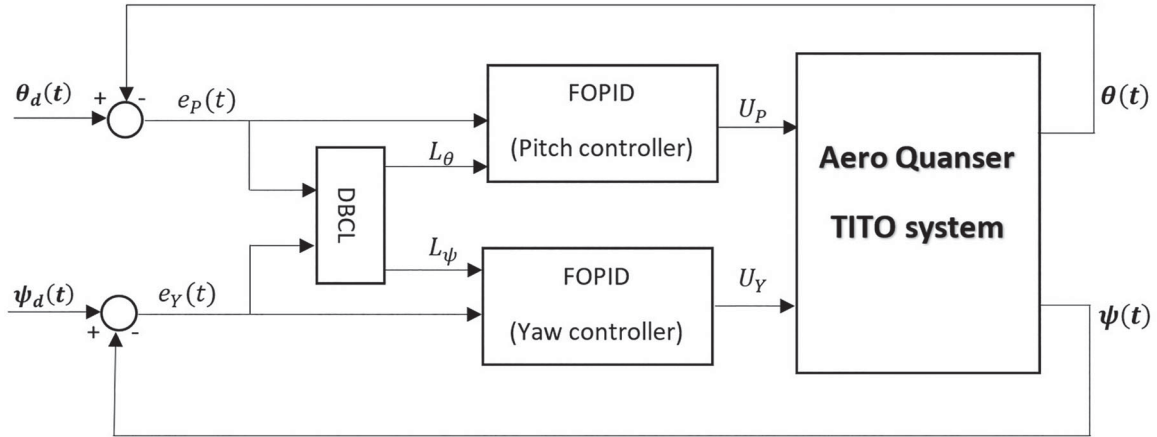


**Figure 5.** FOPID-based DBCL for Quanser Aero control.

overcome this problem, the Dual-Boundary Conditional Law (DBCL) (Haruna et al., 2020) is used because state-space errors can be eliminated using integral control action. DBCL provides a relationship between pitch and yaw errors and the integral control parameters and is mathematically given by (15)

$$L_i(t) = \begin{cases} 0, & |z_i| > t_i > \kappa_i \\ L_{ri}, & t_i \geq |z_i| > \kappa_i \\ L_{ri} + \int \operatorname{sgn}(z_i) & |z_i| \leq \kappa_i t < t_p \\ (\varsigma_{Li}|z_i| + \varsigma_{ri}|\dot{x}_{id}|)dt, & \\ L_{ri} + \int (\varsigma_{Li}|z_i| + \varsigma_{ri}|\dot{x}_{id}|)dt, & |z_i| \leq \kappa_i t \geq t_p \end{cases} \quad (15)$$

where  $i$  takes values of  $\theta$  and  $\psi$ .  $z_i$  is the tracking error of the pitch and yaw angles respectively (i.e.  $z_\theta = e_p$  and  $z_\psi = e_y$ ),  $0 \leq L_{ri} \leq L_{mi}$  where  $L_{mi}$  represents the minimum integral gain required for tracking.  $\kappa_i$  and  $t_i$  denote the widths of the outer and inner boundary layers respectively.  $\varsigma_{Li}$  and  $\varsigma_{ri}$  are positive constants and  $t_p$  denotes the time at which the initial peak occurs in the reference input during the transition phase. The control scheme of the proposed controller-based dual law is illustrated in Figure 5.

### 3.3. RBF neural network

A RBFNN is a neural network used to express a relationship between  $n$  input dimensions and  $m$  output dimensions. This type of neural network uses radial basis functions to model the nonlinear relationships between inputs and outputs. In an  $n$ -dimensional network, the input is directly connected to a hidden layer, where each neuron is defined by an activation function that depends on the Euclidean distance between the input and a vector of dimension  $n$  (Luo, 2019). Each hidden neuron has a unique parameter vector. The output from each neuron in the hidden layer is then multiplied by a weight and transmitted to the output layer. These weights are then updated using the backpropagation or gradient descent method in each iteration. The network outputs are the sum of the neurons in the hidden layer multiplied by their corresponding weights as given in (16). Figure 6 shows the architecture of a RBFNN.

$$\hat{y}_j = \sum_{i=1}^l w_{ij} h_i(\mathbf{X}) \quad (16)$$

where  $h_i$  is the activation function,  $w_{ij}$  the weight parameters and  $\hat{y}_j$  is the neuron output.  $\mathbf{X} = \{x_1, x_2, x_3, \dots, x_m\}^T$  is the  $n$ -dimensional input layer vector. The RBF is expressed

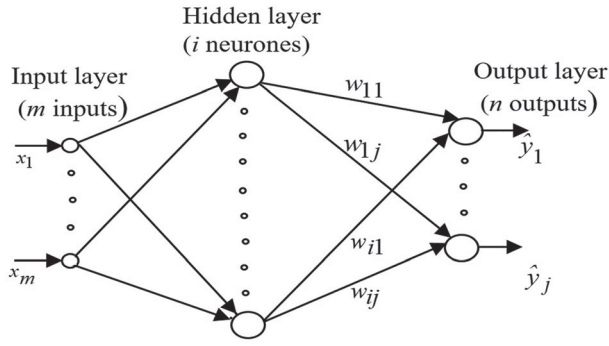


**Figure 6.** RBFNN architecture.

by Gaussian function as

$$h_i(X) = \exp \left[ -\frac{X - C_j^2}{2b_j^2} \right] \quad (17)$$

where  $C_j$  is the centre value of the  $j$ th node  $j = 1, 2, \dots, m$ .  $b_j = [b_1, b_2, \dots, b_m]^T$  and  $W = [w_1, w_2, \dots, w_m]^T$  are the basis vector and weight vector of the network respectively. From (16), the output layer can be given as  $\hat{y}_j = w_1 h_1 + w_2 h_2 + w_3 h_3 + \dots + w_m h_m$ .

In order to adjust the RBFNN, the usual index function  $J$  is given as

$$J = \frac{1}{2} [y - y_d]^2 = \frac{1}{2} e(t)^2 \quad (18)$$

In (18),  $y$  is the output of the controlled system,  $y_d$  is its reference. To minimize  $J$ , the parameters of the output weight, centre vector and basis-width vector are given as follows (Wang et al., 2018):

Output weight:

$$\begin{aligned} \dot{w}_{ij} &= -\eta_w \frac{\partial J}{\partial w_{ij}} \\ &= -\eta_w \frac{\partial J}{\partial e} \frac{\partial e}{\partial y} \frac{\partial y}{\partial w_{ij}} \end{aligned} \quad (19)$$

Centre vector:

$$\begin{aligned} \dot{C}_{ij} &= -\eta_c \frac{\partial J}{\partial C_{ij}} \\ &= -\eta_c \frac{\partial J}{\partial e} \frac{\partial e}{\partial y} \frac{\partial y}{\partial C_{ij}} \end{aligned} \quad (20)$$

Width vector:

$$\begin{aligned} \dot{b}_j &= -\eta_b \frac{\partial J}{\partial b_j} \\ &= -\eta_b \frac{\partial J}{\partial e} \frac{\partial e}{\partial y} \frac{\partial y}{\partial b_j} \end{aligned} \quad (21)$$

where  $\eta_w$ ,  $\eta_c$  and  $\eta_b$  are real positive learning rates.

## 4. Control optimization

In this section, the proposed FGWO algorithm is described in detail. In addition, GWO variants are compared in simulation using benchmark functions to characterize the control performance.

### 4.1. Grey wolf optimization (GWO)

Grey wolves are predators that are ranked at the highest level in the animal food chain. Wolves generally live in packs under strict hierarchical social rules. The GWO optimization method is relatively new and is inspired by the hunting behaviour of wolves and their social hierarchy. The GWO algorithm offers robust convergence compared with other metaheuristic algorithms (Choubey & Ohri, 2022). In this algorithm, the wolves (agents) are organized into four subgroups denoted as alpha ( $\alpha$ ), beta ( $\beta$ ), delta ( $\delta$ ) and omega ( $\omega$ ) (Figure 7).  $\alpha$  is the leader of the pack which typically consists of one or two wolves. Alpha's mission is to make important decisions such as selecting where to sleep, deciding on how long to walk and choosing when to hunt.  $\beta$  is the subordinate of  $\alpha$  and its main task is to help  $\alpha$  in accomplishing the missions.  $\delta$  wolves occupy the third position and are responsible for assisting the  $\beta$  wolves. Finally,  $\omega$  wolves represent the last category of the group with no role assigned to them. Wolves' survival depends on their ability to hunt and find food. To accomplish this goal, wolves must be organized with a high degree of efficiency while adapting to their environment. A typical mission involves encircling, hunting and subsequently attacking the prey. The optimization approach using the GWO algorithm can be summarized as follows: (i) The problem under consideration must be formulated mathematically with parameter initialized. (ii) Randomly initialize the grey wolf pack in the search area. (iii) Dominant wolves  $\alpha$ ,  $\beta$ , and  $\delta$  take charge of leading the pack to search, pursue and encircle prey. Once the prey is surrounded, the search ends and the attack starts.

The life of wolves is based on hunting operation, which is realized in two phases: exploration and exploitation. The former phase is aimed at researching a prey while the later phase involves encircling, hunting, and attacking the prey. The exploration and exploitation behaviours are mathematically indicated by parameters  $\vec{A}$  (22) and  $\vec{C}$  (23) respectively.

$$\vec{A} = 2r_1\vec{a} - \vec{a} \quad (22)$$

where  $\vec{a} = 2 \left( 1 - \frac{\text{actual\_iteration}}{\text{max\_iteration}} \right)$ .

$$\vec{C} = 2r_2 \quad (23)$$

where  $r_1$  and  $r_2$  are random values in the range  $[0, 1]$ .  $\vec{a}$  is a linear parameter, which decreases from two to zero.

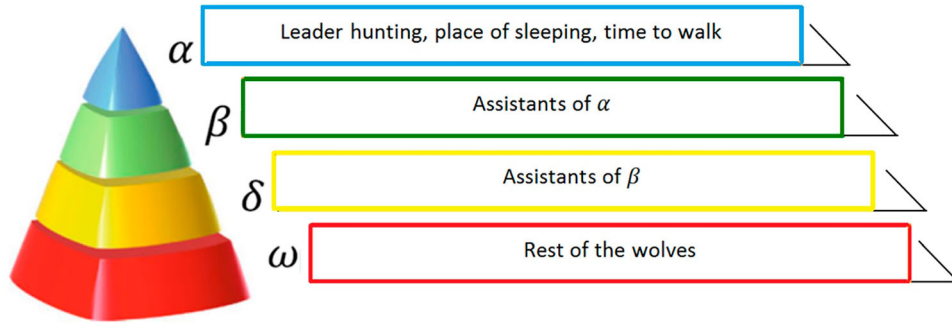


**Figure 7.** Positions and roles within a group of wolves.

**Exploration:** This phase starts when  $|A| > 1$ . The purpose of  $\vec{C}$  is to move the algorithm out of the local minima in the case of stagnation.

**Exploitation:** This phase starts if  $|A| < 1$ .

*Encircling:* This behaviour can be modelled with the following relationship

$$\vec{D} = |\vec{C}\vec{X}_p(t) - \vec{X}(t)| \quad (24)$$

$$\vec{X}(t+1) = \vec{X}_p(t) - \vec{A}\vec{D} \quad (25)$$

where the position vector of the grey wolf is denoted by  $\vec{X}$ .  $\vec{X}_p(t)$  represents the position vector of the prey at the current iteration  $t$ .

*Hunting:* The hunting behaviour is modelled mathematically by

$$X(t+1) = \frac{X_1(t) + X_2(t) + X_3(t)}{3} \quad (26)$$

where  $\vec{X}$  denotes the position of the victim.  $\vec{X}_1$ ,  $\vec{X}_2$  and  $\vec{X}_3$  denote the locations of the  $\alpha$ ,  $\beta$  and  $\delta$  wolves respectively. The  $\alpha$ ,  $\beta$  and  $\delta$  wolves guide the pack towards the  $\omega$  wolves to pursue and ultimately encircle the prey. To define encircling behaviour, three coefficients are suggested for both  $\vec{C}$  and  $\vec{D}$ :

$$\begin{aligned} \vec{D}_\alpha &= |\vec{C}_1\vec{X}_\alpha(t) - \vec{X}(t)|, & \vec{D}_\beta &= |\vec{C}_2\vec{X}_\beta(t) - \vec{X}(t)| \\ \vec{D}_\delta &= |\vec{C}_3\vec{X}_\delta(t) - \vec{X}(t)| \\ \vec{X}_1(t) &= \vec{X}_\alpha(t) - \vec{A}_1\vec{D}_\alpha, & \vec{X}_2(t) &= \vec{X}_\beta(t) - \vec{A}_2\vec{D}_\beta, \\ \vec{X}_3(t) &= \vec{X}_\delta(t) - \vec{A}_3\vec{D}_\delta \end{aligned} \quad (27)$$

The main phases of hunting include encircling and finally attacking a prey.

**Attacking prey:** Once the prey is fixed (prey stops moving), the grey wolves initiate the attack, which is modelled by the  $\vec{A}$ . If  $|A| < 1$  its value will decrease with the increase in  $\vec{a}$  (22).

#### 4.2. Whale optimization algorithm (WOA)

The hunting behaviour of whales is fascinating and simple at the same time. Typically, the prey consists of small

groups of fish. Whales follow the prey near the sea surface by generating bubbles. The hunting behaviour of whales has been modelled in Mirjalili and Lewis (2016) using the Whale Optimization Algorithm (WOA). While WOA shares some similarities with the GWO, it distinguishes itself by employing a spiral approach to replicate the attack phase. The hunting strategy of whales involves three key steps: surrounding prey, executing a spiral bubble net feeding manoeuvre and searching for additional prey. In WOA, unlike GWO, the global optimum is not predetermined; rather, the prey represents the best accepted optimal solution. The positions of the population are adjusted towards the optimal solution as outlined in (28) and (29).

$$\vec{D} = |\vec{C} \times \vec{X}_*(t) - \vec{X}(t)| \quad (28)$$

$$\vec{X}(t+1) = \vec{X}_*(t) - \vec{A} \times \vec{D} \quad (29)$$

where  $D$  is the Euclidean distance between a whale and its prey.  $t$  and  $t+1$  denote the current and subsequent iterations respectively.  $X$  refers to the whale's position vector and  $X_*(t)$  represents the best position at the current iteration and is continuously adjusted with each iteration.  $A$  and  $C$  are vectors determined using (22) and (23) respectively.

The whale's bubble behaviour is mimicked in (30) and (31). In this algorithm, both behaviours such as encircling or spiralling have an equal probability of being utilized; hence, whales choose between them to update their positions as given in (32).

$$\vec{D}' = |\vec{X}_*(t) - \vec{X}(t)| \quad (30)$$

$$X(t+1) = D' e^{bl} \cos(2\pi l) + X_*(t) \quad (31)$$

$$\vec{X}(t+1) = \begin{cases} \vec{X}_*(t) - \vec{A}\vec{D}' & \text{if } p < .5 \\ \vec{D}' e^{bl} \cos(2\pi l) + \vec{X}_*(t) & \text{if } p > .5 \end{cases} \quad (32)$$

where  $p$  is a random number  $[0,1]$ .  $l$  is another random number whose value lies within the range  $[-1,1]$ .  $D'$  denotes the distance of  $i$ th whale by the rapport of the actual prey position, and  $b$  is a constant with a real value.

The exploitation phase involves encirclement and continuous influx of spiral bubbles. Some random moves are also accepted to consider exploration behaviour as given in (33) and (34).

$$\vec{D} = |\vec{C} \times \vec{X}_{\text{rand}}(t) - \vec{X}(t)| \quad (33)$$

$$\vec{X}(t+1) = \vec{X}_{\text{rand}}(t) - \vec{A} \cdot \vec{D} \quad (34)$$

where  $\vec{X}_{\text{rand}}$  is a random position vector (random whale) chosen from the current population.

### 4.3. Ant lion optimizer (ALO)

The ALO was inspired by the hunting strategies of antlion insects. Developed by Mirjalili, it is another nature-inspired optimization algorithm that is used specifically for dealing with continuous optimization challenges (Zatout et al., 2022). As real ants employ stochastic movement patterns to naturally forage for food, ALO adopts a random walk approach to simulate their exploration. ALO emulates the relationship between antlions and ants, such that artificial ants explore the search space while antlions try to capture them. The random walks of the artificial ants are updated according to (35).

$$X_i^t = \frac{(X_i^t - a_i) \times (d_i - c_i^t)}{(d_i^t - a_i)} + c_i \quad (35)$$

where

$$c_i^t = f_t^j + c^t \quad (36)$$

$$d_i^t = f_t^j + d^t \quad (37)$$

where  $X_i^t$  is the position of the ant at iteration  $t$ .  $a_i$  and  $d_i$  respectively represent the minimum and maximum of the  $i$ th variable during random walk.  $c_i^t$  and  $d_i^t$  respectively denote the minimum and maximum of the random walk of the  $i$ th variable at iteration  $t$ .  $c^t$  and  $d^t$  represent the minimum and maximum values among all variables respectively.  $c_j^t$  denotes the minimum value among all variables for the  $i$ th ant,  $d_j^t$  is the maximum value among all variables for the  $i$ th ant,  $f_t^j$  is the position of the chosen  $j$ th antlion for iteration  $t$ .

### 4.4. Fast grey wolf optimization (FGWO)

The central idea of GWO is to redefine the  $\alpha$ ,  $\beta$  and  $\delta$  by assigning them the same importance. However, this is in contradiction with the hierarchical principle of the life of wolves as seen in (26) thus deteriorating the exploration phase. In contrast, the method proposed in this research gives more importance to the leader of the group ( $\alpha$ ), which has a position  $X_1$ . At the same time, the third wolf

will have the least importance. The principle of the proposed FGWO is summarized as follows:

Initially, all the wolves carry the same importance. As the iterations progress,  $X_1$  becomes increasingly important since this position corresponds to the leader and  $X_3$  progressively becomes less important. This behaviour is mathematically formulated with the prey position estimated using the set of equations given in (38) as

$$\left. \begin{aligned} X(n+1) &= \frac{\kappa_1(n)X_1 + \kappa_2(n)X_2 + \kappa_3(n)X_3}{3} \\ \kappa_1(n) &= 1 + \varsigma \left(\frac{n}{N}\right)^{p/q} \\ \kappa_2(n) &= 1 \\ \kappa_3(n) &= 1 - \varsigma \left(\frac{n}{N}\right)^{p/q} \end{aligned} \right\} \quad (38)$$

where  $0 < \varsigma < 1$ ,  $n$  is the actual number of iterations,  $N$  is the maximum number of iterations.  $q$  and  $p$  are integers with  $p > q$ .

**Remark 4.1:** It is easy to note that the value of  $\kappa_1$  increases with an increase in the number of iterations, whereas the value of  $\kappa_3$  decreases in each iteration. In addition, the weights  $\kappa = (\kappa_1, \kappa_2, \kappa_3)$  must satisfy the condition given in (39) as

$$\kappa_1 + \kappa_2 + \kappa_3 = 3 \quad (39)$$

The condition (39) also holds true in the case of GWO.

In their real hunting process, the leading wolves ( $\alpha$ ,  $\beta$  and  $\delta$ ) will never be at the same distance from the victim since  $\alpha$  wolf always advances compared to  $\beta$  and  $\delta$  wolves. At the same time,  $\beta$  is always advanced compared to  $\delta$ . In other words,  $X(n+1)$  is close to  $\alpha$ , medium to  $\beta$  and far to  $\delta$ . Therefore, it is important to estimate the optimal position of the victim. Figure 8 illustrates that  $\alpha$  wolf enters a circle closer to the victim, sequentially followed by  $\beta$ ,  $\delta$  and finally the  $\omega$  wolves. It is clear that this order is followed in the wolf community. These differences in distances are modelled by the function  $\kappa_i(n)$  ( $i = 1, 2, 3$ ).  $\kappa_2(n) = 1$  is considered a constant, this indicates that  $\kappa_1(n) = 1 + \varsigma \left(\frac{n}{N}\right)^{p/q}$  will have more importance closer to the prey due to the nonlinear term  $\varsigma \left(\frac{n}{N}\right)^{p/q}$ . At the same time,  $\delta$  loses importance with the progression of  $n$  owing to the term  $-\varsigma \left(\frac{n}{N}\right)^{p/q}$  of the function  $\kappa_3(n)$ . These functions in the proposed FGWO offer a more exact estimation of  $X(n+1)$  compared to the GWO method. The new method is given by (27) and (38). GWO and FGWO algorithms are depicted in Figures 9 and 10 respectively.

**Remark 4.2:** The values of  $\varsigma$ ,  $q$  and  $p$  are determined through trial and error.

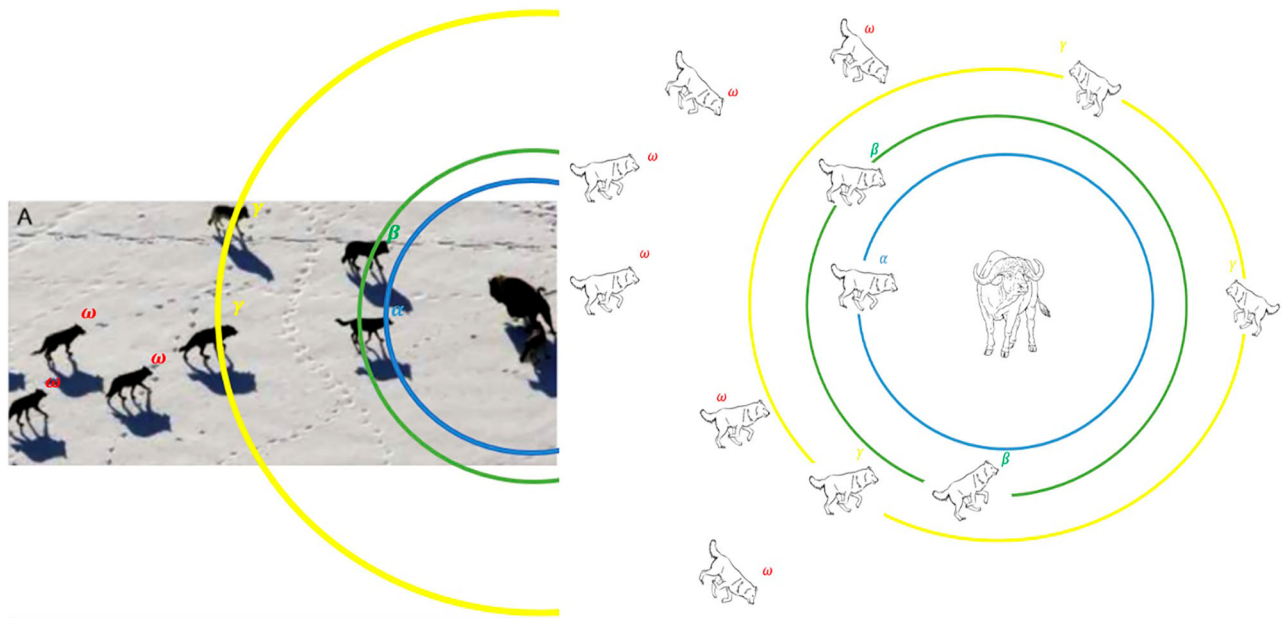


Figure 8. FGWO principle.

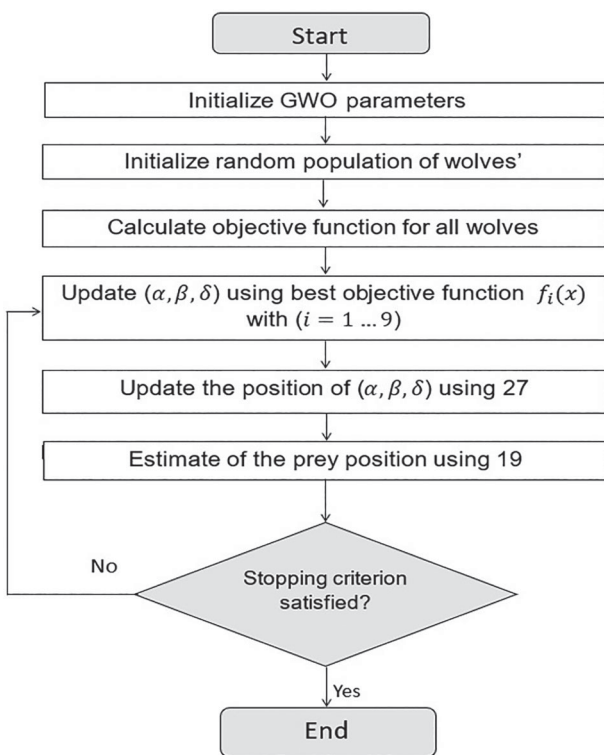


Figure 9. GWO algorithm.

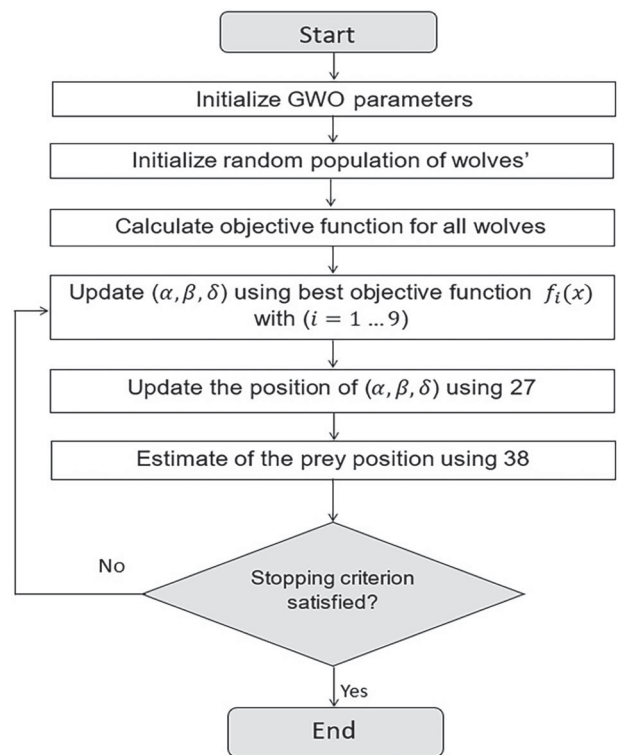


Figure 10. Proposed FGWO algorithm.

### 5. Dual-RBFNN-FOPID-FGWO (DRF-FG) design

In this section, the designs of FOPID, FGWO-FOPID, and DRF-FG are detailed. In the first step, FOPID parameters are optimized using GWO and FGWO algorithms. In the second step, RBFNN controllers are involved to vary each parameter of FOPID.

#### 5.1. FGWO-FOPID design

The first step pertinent to system control is the optimization of the FOPID controller using GWO and its variants. The objective function in this study is a combination of two performance measures: the Integral of Time-weighted Absolute Error (ITAE) and the Integral Squared

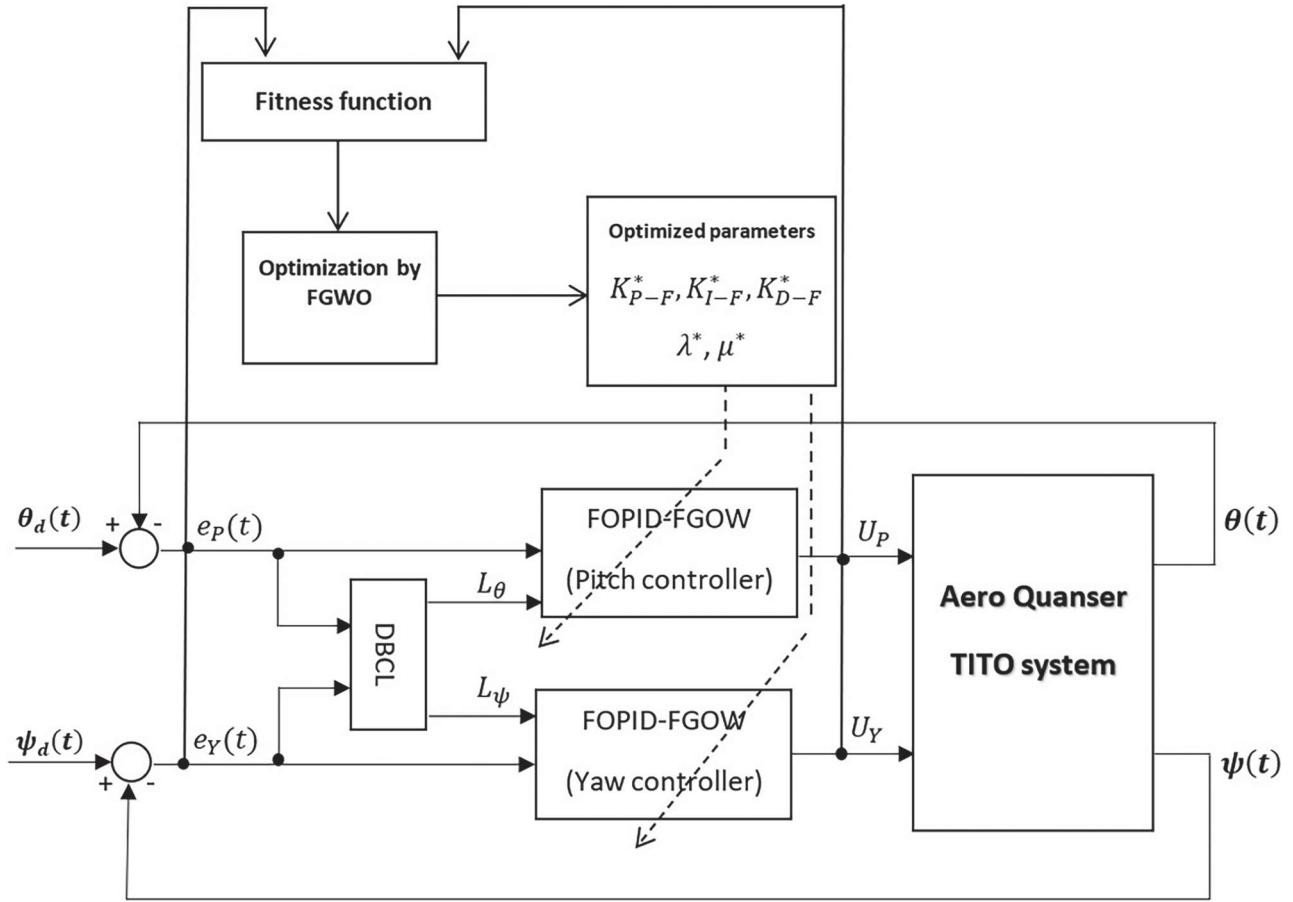


**Figure 11.** FOPID controller based on FGWO.

Control (ISC). The ITAE-based objective offers specific advantages: (i) it aims to minimize time to achieve stability and (ii) it reduces the maximum overshoot by multiplying time with the absolute error. On the other hand, ISC aims to prevent excessive control effort that could potentially impair the system's actuators. Moreover, ISC optimizes energy consumption within the system. The proposed fitness function is named as IATESC. This function is calculated at each iteration and for each agent (wolf), subject to the step response. Figure 11 illustrates the optimization procedure.

The objective function is formulated by combining Integral Time-weighted Absolute Error (ITAE) and Integral Squared Control (ISC) and is abbreviated as IATESC given in (40).

$$J(e, u) = \int_{t_0}^{t_f} (t^T H |e| + u^T M u) dt \quad (40)$$

where the matrix  $H \in R_+^{2 \times 2}$  is chosen to guarantee precision, robustness and minimum time to achieve stability. The matrix  $M \in R_+^{2 \times 2}$  ensures that the control inputs do

not exceed their maximum values. Thus  $M$  can safeguard system actuators.  $e_\varphi = \varphi_d - \varphi$  is the pitch error,  $e_\psi = \psi_d - \psi$  is the yaw error.  $t_0$  and  $t_f$  represent the initial and final times respectively.

The control law (14) becomes

$$\left. \begin{aligned} u(t) &= K_{P-FG} e(t) + K_{I-FG} \int_{t_0}^{t_f} e(t) dt^\lambda + K_{D-FG} \frac{d^\mu e(t)}{dt^\mu} \\ U(S) &= \left( K_{P-FG} + \frac{K_{I-FG}}{S^\lambda} + K_{D-FG} S^\mu \right) E(S) \end{aligned} \right\} \quad (41)$$

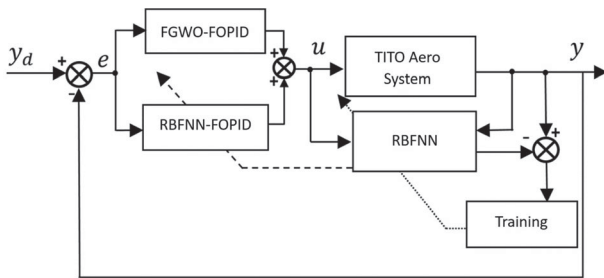
## 5.2. DUAL-RBFNN-FOPID-FGWO (DRF-FG) controller

The parameter tuning of the FGWO-FOPID controller is done using RBFNN. The newly proposed DRF-FG control can be expressed as follows:

$$\left. \begin{aligned} K_{P-NN}^* &= K_{P-FG}^* + \Delta K_{P-NN} \\ K_{I-NN}^* &= K_{I-FG}^* + \Delta K_{I-NN} \\ K_{D-NN}^* &= K_{D-FG}^* + \Delta K_{D-NN} \end{aligned} \right\} \quad (42)$$

**Table 2.** Used fitness benchmark functions.

Function	Dim	Range	$f_{\min}$
$f_1(x) = \sum_{i=1}^n x_i^2$	30	[-100, 100]	0
$f_2(x) = \sum_{i=1}^n  x_i  + \prod_{i=1}^n  x_i $	30	[-10, 10]	0
$f_3(x) = \sum_{i=1}^n \left( \sum_{j=1}^i x_j \right)^2$	30	[-100, 100]	0
$f_4(x) = \max_{x_i} \{ x_i , 1 \leq i \leq n\}$	30	[-100, 100]	0
$f_5(x) = \sum_{i=1}^{n-1} [100(x_{i+1} - x_i^2)^2 + (x_i - 1)^2]$	30	[-30, 30]	0
$f_6(x) = \sum_{i=1}^n (x_i + 0.5)^2$	30	[-100, 100]	0
$f_7(x) = \sum_{i=1}^n ix_i^4 + \text{random}[0, 1]$	30	[-1.28, 1.28]	0
$f_8(x) = \sum_{i=1}^n [x_i^2 - 10 \cos(2\pi x_i) + 10]$	30	[-5.12, 5.12]	0
$f_9(x) = -20 \exp\left(-0.2 \sqrt{\frac{1}{n} \sum_{i=1}^n (x_i)^2}\right) - \exp\left(\frac{1}{n} \sum_{i=1}^n 10 \cos(2\pi x_i)\right) + 20 + e$	30	[-32, 32]	0


**Figure 12.** Proposed DRF-FG control scheme.

Thus (41) becomes,

$$\left. \begin{aligned} u(t) &= K_{P-NN}^* e(t) + K_{I-NN}^* \int_{t_0}^{t_f} e(t) dt^\lambda + K_{D-NN}^* \frac{d^\mu e(t)}{dt^\mu} \\ U(S) &= \left( K_{P-NN}^* + K_{I-NN}^* \frac{1}{S^\lambda} + K_{D-NN}^* S^\mu \right) E(S) \end{aligned} \right\} \quad (43)$$

The tuned DRF-FG parameters are  $K_{P-NN}^*$ ,  $K_{I-NN}^*$  and  $K_{D-NN}^*$  and the final control law is given by (43). The control block diagram of the proposed DRF-FG is illustrated in Figure 12.

From an algorithmic point of view, the proposed DRF-FG controller for the Quanser Aero system is realized in a hierarchical manner. Initially, a decentralized classical FOPID control law has been developed, which is followed by the design of a FOPID-FGWO. Finally, DRF-FG is realized.

**Remark 5.1:** It is imperative to indicate that the RBFNN allows for having an adaptive control law owing to flexibility and ability of quick processing of RBFNN compared to the conventional NN or deep neural networks.

The proposed controller is simple (due to FOPID part), optimal (owing to the use of the proposed FGWO) and adaptive (thanks to RBFNN capabilities). The use of the proposed controller for large classes of nonlinear systems is possible because it does not necessarily involve modelling of the system to be controlled.

## 6. Simulation results

### 6.1. FGWO validation

Simulations are conducted to determine the optimal values of the control parameters and to characterize the control performance. Simulations are performed in MATLAB/Simulink 2021a environment running on a laptop HP Pavilion with AMD E1-6010APU processor, AMD Radeon R2 Graphics card and 1.35 GHZ processor and 8 GB RAM. The effectiveness of the proposed FGWO is demonstrated using nine benchmark test functions, which are listed along with their properties in Table 2.

For a meaningful comparison between GWO and FGWO, we used the same number of iterations, dimensions (D) and agents. These values are as follows: iterations = 1000,  $D = 30$  and agents = 30. We performed a set of tests (30 tests) using different values of  $p$  and  $q$  which are summarized in Table 3. The value of  $\zeta$  is chosen to be 1 i.e.  $\zeta = 1$ . The variants of GWO are named GWO\_ $q/p$  with variations in  $p$  and  $q$ . In this regard, we obtain GWO\_1, GWO\_1/2, GWO\_1/3, and GWO\_1/4. The results obtained after 30 independent runs are presented in Table 4. Numerical and graphical comparisons of these variants are given in Figure 13 depicting that the proposed variant FGWO depicted superior performance.

From Figure 13(a–d,g–i), we deduce that GWO\_1/3 offers the best results since it quickly approaches to the

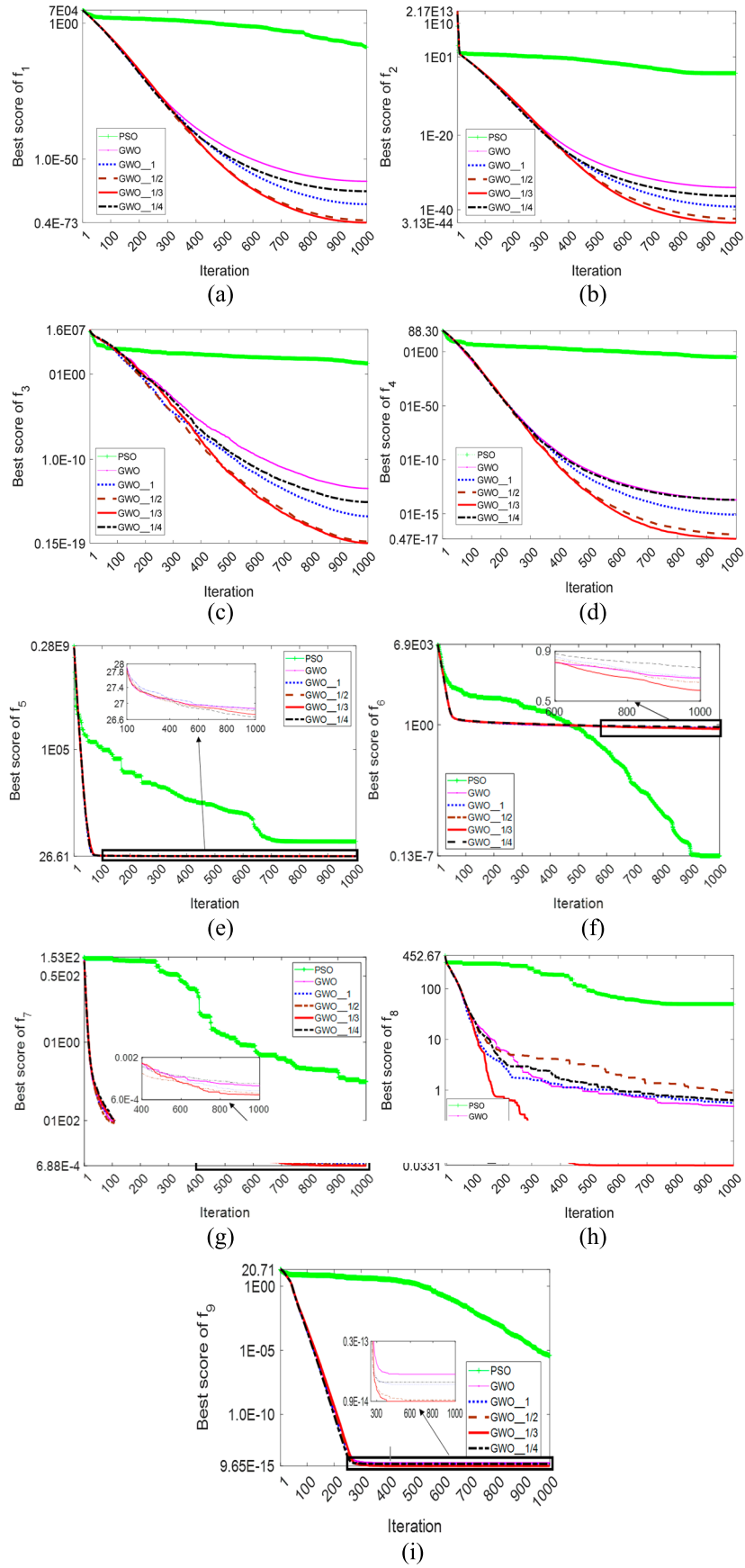


**Figure 13.** Results of comparison of PSO, GWO and its variant. (a)  $f_1$ , (b)  $f_2$ , (c)  $f_3$ , (d)  $f_4$ , (e)  $f_5$ , (f)  $f_6$ , (g)  $f_7$ , (h)  $f_8$  and (i)  $f_9$ .

**Table 3.** Parameters used for improving GWO.

Experiences	$q$	$p$	Variant name
E1	0	1	GWO
E2	1	1	GWO_1
E3	1	2	GWO_1/2
E4	1	3	GWO_1/3
E5	1	4	GWO_1/4

minimum compared to the other variants. GWO\_1/3 variant provides best results in the majority of cases except ones illustrated in Figure 13(e–f). PSO demonstrates best performance only in the case of Figure 13(f) with the fitness function  $f_6$ . The superior performance of PSO compared to GWO in Figure 13(f) can be attributed to the fact that, in PSO, exploitation is more effective when searching for the optimum. The better result can be explained by the nature of the objective function; the optimum of this function is shifted by 5. In contrast to PSO, GWO is based on leadership and requires an accurate balance between exploitation and exploration. The optimal solution is close to the original optimal solution as reported in Yang et al. (2024). In Mirjalili et al. (2014), the same result was obtained. In Figure 13(e) (i.e.  $f_5$ ), the best result is given by GWO\_1/4, though the difference between this result and the results demonstrated by other variants is negligible. From a fast convergence point of view, the proposed approach offers the best robustness in  $f_1, f_2, f_3, f_4, f_7, f_8$  and  $f_9$  cases, even though these functions are not always the best at the beginning of the optimization. In addition, a very important conclusion can be drawn that in all the cases, GWO\_1/3 performed better than the classical GWO for any fitness function. The detailed results achieved are presented in Table 4.

The numerical performance comparison presented in Table 4 lists the best, mean, and worst values of the benchmark fitness functions. In addition, the rank of each variant is given and the standard deviation is shown. These results evidence the superior performance of GWO\_1/3 in providing a solution closer to the valid optimum value for  $f_1, f_2, f_3, f_4, f_7, f_8$  and  $f_9$ . This remarkable performance offered by GWO\_1/3 can be explained by the maximum influence associated with the leadership of the group i.e.  $X_1$  and simultaneously assigning the minimum weight to  $X_3$ . From the best, mean and worst values of  $f_1, f_2, f_3, f_4, f_7, f_8$  and  $f_9$ , we can see the gradual improvement in finding the minimums of these objective functions from GWO to GWO\_1/3, i.e. GWO\_1 gives better results than GWO, GWO\_1/2 gives better results than GWO\_1 and so on. However, after this, GWO\_1/4 achieved worse results than GWO\_1/3. In addition, although functions  $f_7, f_8$  and  $f_9$  are characterized as local minima, GWO\_1/3 also demonstrated the best results with these fitness functions. This observation

allows us to conclude that the best values of  $p$  and  $q$  are  $p = 1$  and  $q = 3$ . Thus, (38) can be rewritten as:

$$\left. \begin{aligned} X(n+1) &= \frac{\kappa_1(n)X_1 + \kappa_2(n)X_2 + \kappa_3(n)X_3}{3} \\ \kappa_1(n) &= 1 + \left(\frac{n}{N}\right)^{1/3} \\ \kappa_2(n) &= 1 \\ \kappa_3(n) &= 1 - \left(\frac{n}{N}\right)^{1/3} \end{aligned} \right\} \quad (44)$$

It can be observed that GWO\_1/4 demonstrated the best performance for the fitness functions  $f_5$  and  $f_6$ . These results confirmed a shortcoming in the GWO algorithm in terms of its premature convergence to the minimum. It is also noted that improvement in GWO and GWO\_1/4 is negligible in the case of the fitness function  $f_6$  and the same remark can be made for GWO\_1/4 and GWO\_1/3 in the case of  $f_5$ . In all cases, GWO\_1/3 offered the best results compared with the classical GWO. Since GWO\_1/3 is the best, it is named as FGWO. These results are confirmed by conducting simulations using a mean of 30 tests and are illustrated in Figure 13.

## 6.2. FOPID-FGWO controller for the Quanser Aero system

This subsection presents the optimization of FOPID based on the FGWO algorithm. The FOPID-FGWO controller is compared with FOPID-GWO, FOPID-WOA, and FOPID-ALO controllers. WOA and ALO algorithms are introduced for several reasons: (i) These algorithms are more recent than GWO (ii) In some scientific works, ALO and/or WOA are reported to perform better than GWO, thus the objective to include them here is to evaluate if the proposed FOPID-FGWO outperforms than these algorithms (iii) Also, these algorithms do not bear the same hierarchical characteristics compared to GWO. The objective function IATESC (40) must be optimized. Ten experiences are carried out with 50 iterations of each test for all the controllers. Figure 14 illustrates the simulated IATESC fitness profile obtained from the design of the FOPID controller. The result on the minimal of the IATESC function indicates that compared to FOPID based on GWO, ALO and WOA, FGWO demonstrates robust convergence since it converges to the minimum after 38 iterations with 10 separate tests. GWO suffers premature convergence to the minimum after only 11 iterations. These results confirm the superiority of FGWO compared to the other FOPID algorithms based on GWO, ALO and WOA. The fitness curvature of FGWO started from 4.15482 (i.e. the value of the fitness function at iteration 1), which is more than that the corresponding value in ALO. The minimum is

**Table 4.** Results of the benchmark functions (**bold** numbers indicate the optimal values closer to the global minimal).

Function	Variants of GWO	Best	Mean	Worst	St. dev.	Rank
$f_1(x)$	GWO	8.0124e - 62	7.5319e - 59	6.1035e - 58	2.8409e + 03	5
	GWO_1	6.1760e - 71	1.7692e - 67	2.6598e - 66	2.8581e + 03	3
	GWO_1/2	3.5084e - 76	1.3051e - 73	1.5145e - 72	1.0591e + 05	2
	GWO_1/3	<b>3.3182e - 78</b>	<b>6.4085e - 75</b>	<b>4.8075e - 74</b>	1.0647e + 05	1
	GWO_1/4	2.3074e - 65	8.9827e - 63	6.6215e - 62	1.0360e + 05	4
$f_2(x)$	GWO	4.2423e - 36	9.5003e - 35	3.0491e - 34	2.2072e + 08	5
	GWO_1	3.5217e - 41	6.9913e - 40	3.8734e - 39	4.3240e + 07	3
	GWO_1/2	7.5532e - 45	4.0721e - 43	5.2700e - 42	2.0625e + 13	2
	GWO_1/3	<b>8.5130e - 46</b>	<b>3.1290e - 44</b>	<b>1.5617e - 43</b>	3.9900e + 12	1
	GWO_1/4	1.0485e - 38	4.8375e - 37	2.0205e - 36	2.3742e + 12	4
$f_3(x)$	GWO	4.9019e - 21	3.9956e - 14	6.1747e - 13	7.0243e + 03	5
	GWO_1	1.2563e - 22	2.1708e - 17	4.0484e - 16	5.9440e + 03	3
	GWO_1/2	2.5343e - 24	2.4174e - 20	2.9473e - 19	2.6382e + 05	2
	GWO_1/3	<b>2.4043e - 25</b>	<b>1.5364e - 20</b>	<b>2.7942e - 19</b>	2.8914e + 05	1
	GWO_1/4	1.3620e - 22	1.0091e - 15	2.5420e - 14	2.7740e + 05	4
$f_4(x)$	GWO	3.1364e - 16	1.9444e - 14	9.1717e - 14	7.0988	5
	GWO_1	9.3433e - 18	8.2577e - 16	6.8860e - 15	7.9913	3
	GWO_1/2	3.1181e - 19	7.6399e - 17	1.2170e - 17	291.4135	2
	GWO_1/3	<b>7.0475e - 20</b>	<b>4.7773e - 18</b>	<b>8.1443e - 17</b>	289.8504	1
	GWO_1/4	2.6882e - 16	1.9345e - 14	1.5531e - 13	294.3609	4
$f_5(x)$	GWO	25.3788	26.8788	28.7581	8.3017e + 06	4
	GWO_1	25.6383	26.8486	28.7279	8.0655e + 06	5
	GWO_1/2	25.2273	26.8187	28.5193	3.5328e + 08	3
	GWO_1/3	25.2145	26.7294	<b>27.9545</b>	3.4873e + 08	2
	GWO_1/4	<b>25.1755</b>	<b>26.6667</b>	28.5396	3.4239e + 08	1
$f_6(x)$	GWO	1.5113e - 05	0.65583	1.5040	2.8720e + 03	2
	GWO_1	7.6671e - 05	0.6617	1.5113	2.7434e + 03	4
	GWO_1/2	0.2447	0.6239	1.5118	1.0443e + 05	5
	GWO_1/3	2.9440e - 05	<b>0.5678</b>	1.7387	1.0303e + 05	3
	GWO_1/4	<b>1.4766e - 05</b>	0.7449	<b>1.4949</b>	1.0236e + 05	1
$f_7(x)$	GWO	1.6840e - 04	0.0089	<b>0.0022</b>	4.2328	4
	GWO_1	1.4976e - 04	7.6915e - 04	0.0026	4.3668	3
	GWO_1/2	1.4767e - 04	7.2028e - 04	<b>0.0022</b>	159.3594	2
	GWO_1/3	<b>1.3329e - 04</b>	<b>6.8861e - 04</b>	0.0023	159.1853	1
	GWO_1/4	2.3297e - 04	9.6009e - 04	<b>0.0022</b>	153.2305	5
$f_8(x)$	GWO	0	4.8367	11.1145	42.7259	5
	GWO_1	0	0.5642	8.6364	46.1779	3
	GWO_1/2	0	0.8826	18.4883	1.5578e + 03	4
	GWO_1/3	<b>0</b>	<b>0.0332</b>	<b>0.9956</b>	1.5573e + 03	1
	GWO_1/4	0	0.6360	10.2670	1.5407e + 03	4
$f_9(x)$	GWO	1.1546e - 14	1.6165e - 14	2.2204e - 14	1.9632	5
	GWO_1	7.9936e - 15	1.3323e - 14	1.5099e - 14	2.1442	2
	GWO_1/2	7.9936e - 15	9.8884e - 15	1.5099e - 14	66.2385	4
	GWO_1/3	7.9936e - 15	9.6515e - 15	1.5099e - 14	66.6093	1
	GWO_1/4	7.9936e - 15	1.3915e - 14	2.2204e - 14	67.1078	3

achieved after 38 iterations, thus establishing the robust convergence of FGWO compared with the other variants.

Table 5 presents IATESC performance after simulating the experiences. From the table, it can be confirmed that in all cases, FGWO demonstrated superior performance, which is followed by GWO and WOA in sequential order of performance. The worst results of the IATESC are achieved by ALO. Quantitatively, FGWO improves IATESC performance by +2.0403% compared with GWO. Marginal improvements of +0.0403% and +1.6067% are demonstrated respectively by GWO and WOA.

The FOPID parameters obtained using the aforementioned optimization methods are summarized in Table 6. These parameters are different for each approach. In order to protect the helicopter actuators in the optimization procedures, saturation was applied on the control signals. This is to simulate physical limitations on

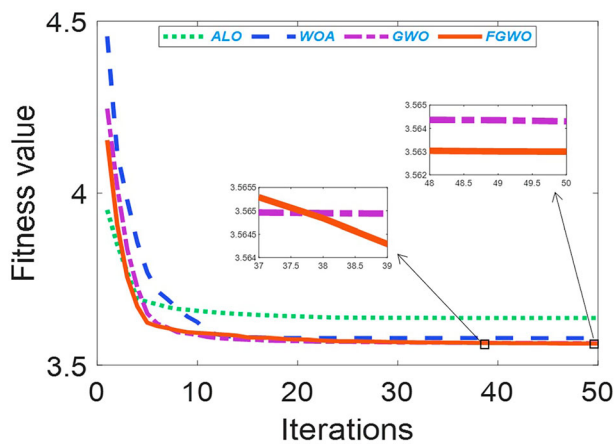
**Table 5.** IATESC performances.

	Best	Average	Worth	Standard deviation
ALO	3.6372	3.6579	3.6948	0.5152
WOA	3.5788	3.6345	3.6654	0.1582
GWO	3.5643	3.6040	3.5914	0.1205
FGWO	<b>3.5630</b>	<b>3.5989</b>	<b>3.5872</b>	<b>0.0981</b>

actuators to void significant deviations from desired performance thus enhancing the reliability of the results obtained. Hence, by simulating these constraints during parameter optimization, one can develop controllers that are effective under real operating conditions. The optimization procedure of the FOPID based on all the meta-heuristic methods involves  $\pm 24$  V saturation for the two actuators of the system. In the next step, the application of the designed controller in trajectory tracking mode is compared.

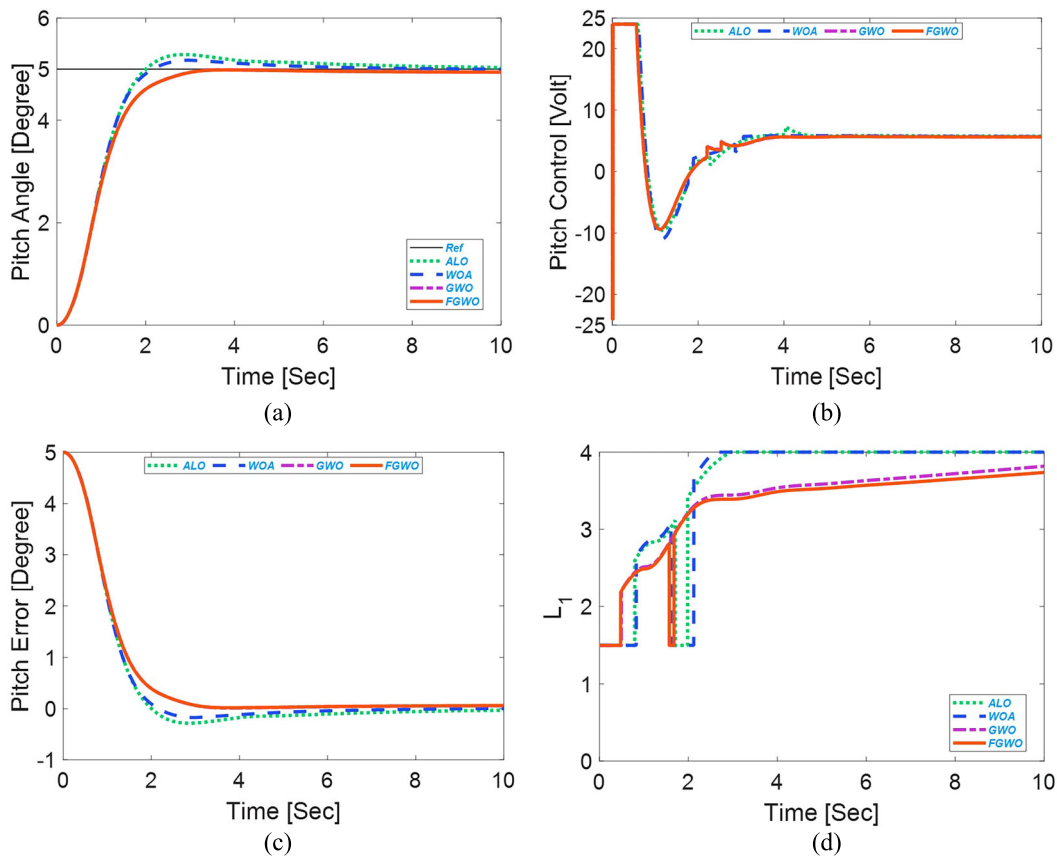
**Table 6.** Optimized FOPID parameters.

	Pitch FOPID parameters					Yaw FOPID parameters				
	$P$	$I$	$D$	$\mu$	$\lambda$	$P$	$I$	$D$	$\mu$	$\lambda$
ALO	40.2191	17.6043	59.7016	0.0443	0.4999	59.9589	41.3310	58.8391	0.3568	0.3613
WOA	49.9992	12.0008	59.9990	1e-10	0.5	59.9990	53.9990	59.9990	0.4491	0.3833
GWO	49.1389	0.5419	59.9994	0.0055	0.5	60	48.2987	60	0.1474	0.2056
FGWO	49.7691	0.3708	60	0.0014	0.5	60	48.2749	60	0.1618	0.1794


**Figure 14.** IATESC profile.

### 6.3. DRF-FG controller for the Quanser Aero system

In the regulation mode, the Quanser Aero system was tested to reach the desired angles  $(\theta_d, \psi_d) = (5, 5)$  degrees in one step. FOPID control parameters, given in Table 6, are used for ALO, WOA, GWO and proposed FGWO. Four control variants (DRF-FG, DRF-G, DRF-W, and DRF-A) are tested and the results obtained are illustrated in Figures 15 and 16. Six RBFNN controllers are used, each of which is composed of a Single-Input and Single-Output (SISO). The number of neurons in the handle layers (N) and their weights are summarized in the table given in Appendix. The weights of the RBFNN are tuned using the (19). The RBFNN parameters are presented in Table A1 given in Appendix. The choice to use more neurons for


**Figure 15.** Simulation results of Dual FOPID RBFNN based on FGWO, GWO, WOA and ALO in regulation mode. (a) Pitch angle, (b) pitch control, (c) pitch error and (d) dual  $L_1$  parameter evolution.

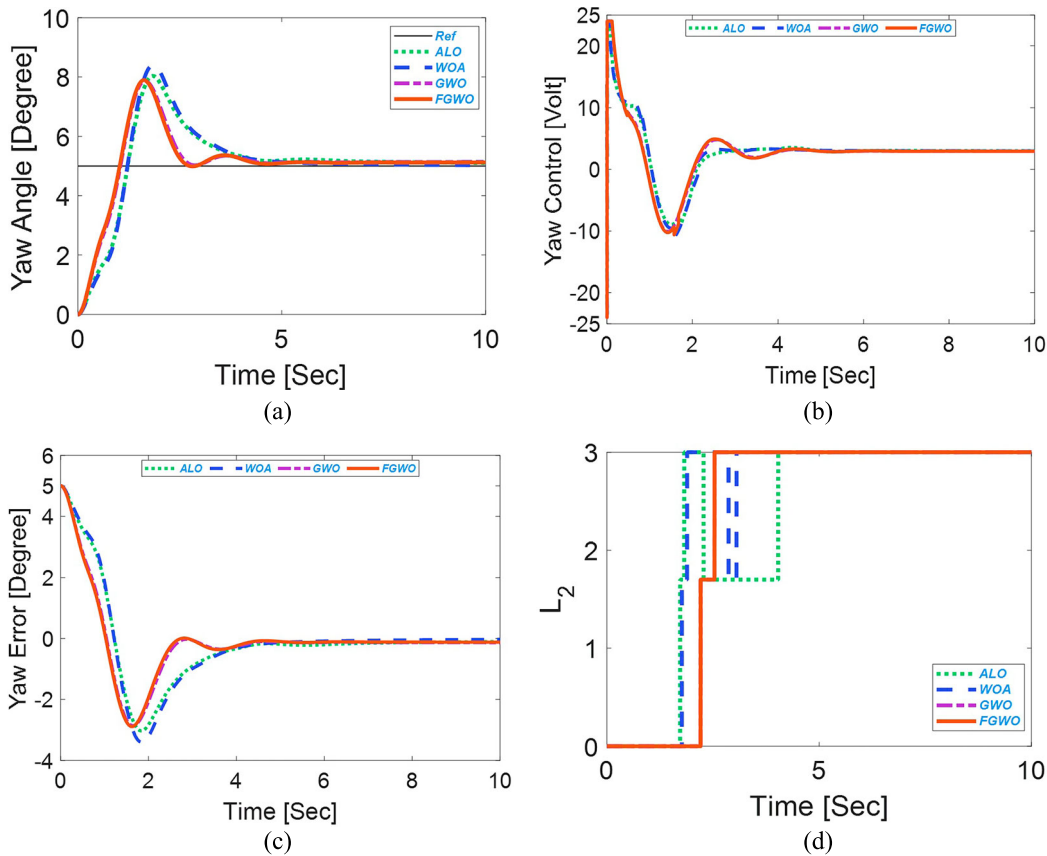


**Figure 16.** Simulation results of Dual FOPID RBFNN based on FGWO, GWO, WOA and ALO in regulation mode. (a) Yaw angle, (b) yaw control, (c) yaw error and (d) dual  $L_2$  parameter evolution.

integral and derivative actions is justified by the objective of dealing with the nonlinearity of the Quanser Aero system. The structure of the RBFNN is obtained by trial and error. The proposed controller is obtained in a hierarchical manner in several key stages. Initially, all the FOPID parameters are optimized by FGWO. In the second stage, RBFNN is used to adjust only the six PID parameters. The third stage involves using the dual approach to improve the precision. This approach will be active only if the system response is closer to the desired trajectory. Dual mechanism is applied only to the two integrators corresponding to the pitch and yaw controllers. The four fractional parameters are adjusted by FGWO. It is pertinent to mention here that RBFNNs have an adaptive role to deal with nonlinearities, uncertainties and dynamical changes in the system. In addition, dual part is used to deal with cross-coupling effect.

Figures 15 and 16 show that DRF-FG achieves the best results. After some oscillations at approximately 2.812 s for the yaw angle and 4.2 s for the pitch angle, the response is stable with practically zero error for all the angles i.e. no oscillations in the control signals are observed afterwards. Since parameters  $L_1$  and  $L_2$  are

related to steady-state errors, their values are zero during the initial transit phase. However, these parameters start to increase progressively during the steady-state phase. In addition, because DRF-FG is the best controller,  $L_1$  does not reach its superior bound. The performance of all the controllers under investigation in the regulation mode is presented in Table 7. From the table, we can remark that, among the eight-performance metrics, the controller based on FGWO demonstrated the best performance w.r.t. the four parameters that include %OS of pitch and yaw angles,  $T_s$  of pitch and  $T_r$  of yaw angles.

**Trajectory tracking:** This simulation involves the trajectory tracking mode to characterize all the approaches under investigation. The selected trajectories are given by (45). FOPID parameters and RBFNN structures used here are the same as those employed in the regulation mode. The angular pitch and yaw and their corresponding control signals, errors and dual adaptive gains  $L_1$  and  $L_2$  are shown in Figures 17 and 18 respectively.

$$\left. \begin{aligned} \psi_d(t) &= 10 \sin(0.1t) \\ \varphi_d(t) &= 10 \sin(0.1t) \end{aligned} \right\} \quad (45)$$

**Table 7.** Regulation mode performance of Dual FOPID RBFNN based on ALO, WOA, GWO and FGWO.

Dual FOPID RBFNN	Pitch angle				Yaw angle			
	%OS [%]	Tr [s]	Ts [s]	SS errors [degrees]	%OS [%]	Tr [s]	Ts [s]	SS errors [degrees]
ALO	2.852%	<b>1.1880</b>	6.196	0.0351	30.348	0.946	–	0.101
WOA	1.7427%	1.2040	4.344	<b>5.3e – 04</b>	33.937	0.932	<b>5.588</b>	<b>0.0296</b>
GWO	0%	1.4620	2.814	0.0570	28.942	0.788	–	0.139
FGWO	<b>0%</b>	1.4600	<b>2.812</b>	0.0591	<b>28.62</b>	<b>0.7720</b>	–	0.134

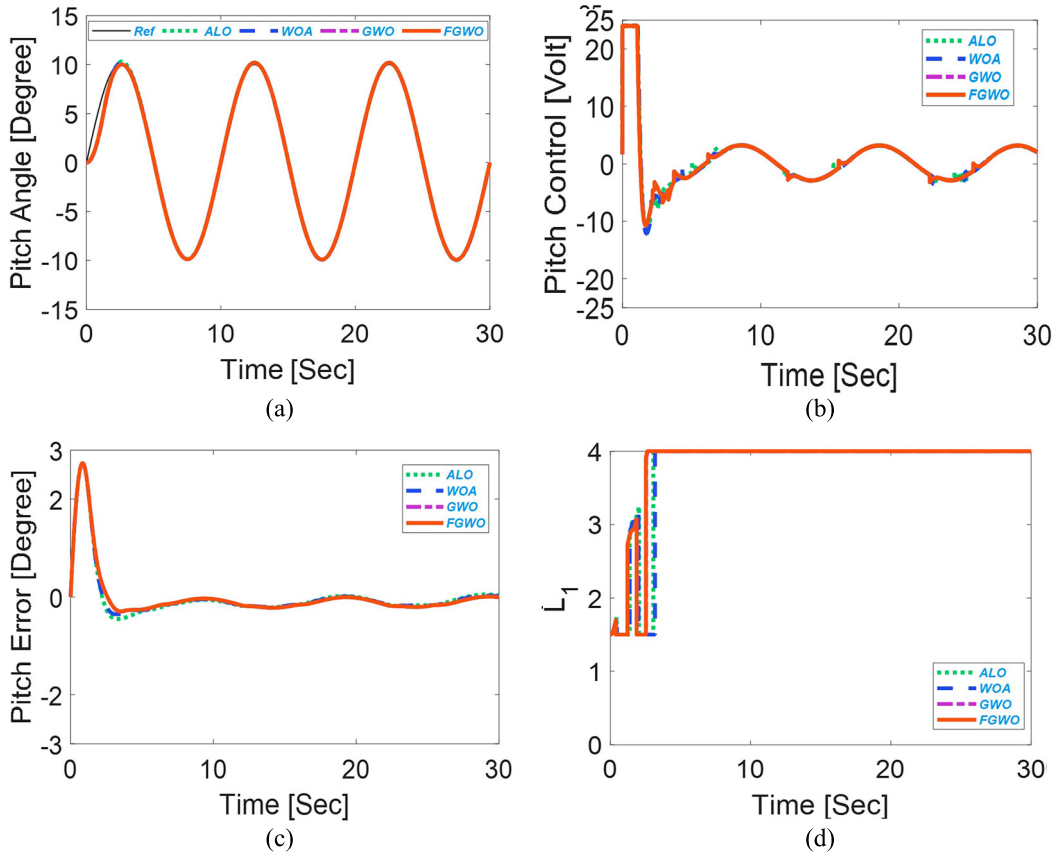


**Figure 17.** Simulation results of Dual FOPID RBFNN based on FGWO, GWO, WOA and ALO in trajectory tracking. (a) Pitch angle, (b) pitch control, (c) pitch error and (d) dual  $L_1$  parameter evolution.

To characterize the performance of the controllers to determine whether the controller demonstrates superior performance, various error parameters are considered in this study. These include Integral Time Absolute Error (ITAE), Integral Squared Error (ISE), Integral Squared Control (ISC), Mean of Average Error (MAE) and Integral Absolute Error (IAE). These criteria are given as (with  $i = \psi, \varphi$ ),

$$ITAE = \int_0^{t_f} t(|e_i(t)|)dt$$

$$ISE = \int_0^{t_f} e_i^2(t)dt$$

$$ISC = \int_0^{t_f} u_i^2(t)dt$$

$$MAE = \frac{1}{t_f} \int_0^{t_f} (|e_i(t)|)dt$$

$$IAE = \int_0^{t_f} |e_i(t)|dt$$

Table 8 summarizes the results achieved corresponding to these error parameters. From the table, it can be inferred that, based on the values of ITAE, ISE, MAE and IAE, the proposed DRF-FG algorithm demonstrates superior performance compared to its counterpart based on DRF-G, DRF-W, and DRF-A algorithms. By forming the sum of the yaw and pitch angles corresponding to the ISE, MAE, IAE and ITAE error metrics, it is confirmed that DRF-FG algorithm overperforms than DRF-G, DRF-W, and DRF-A algorithms. The performance of GWO-based controllers

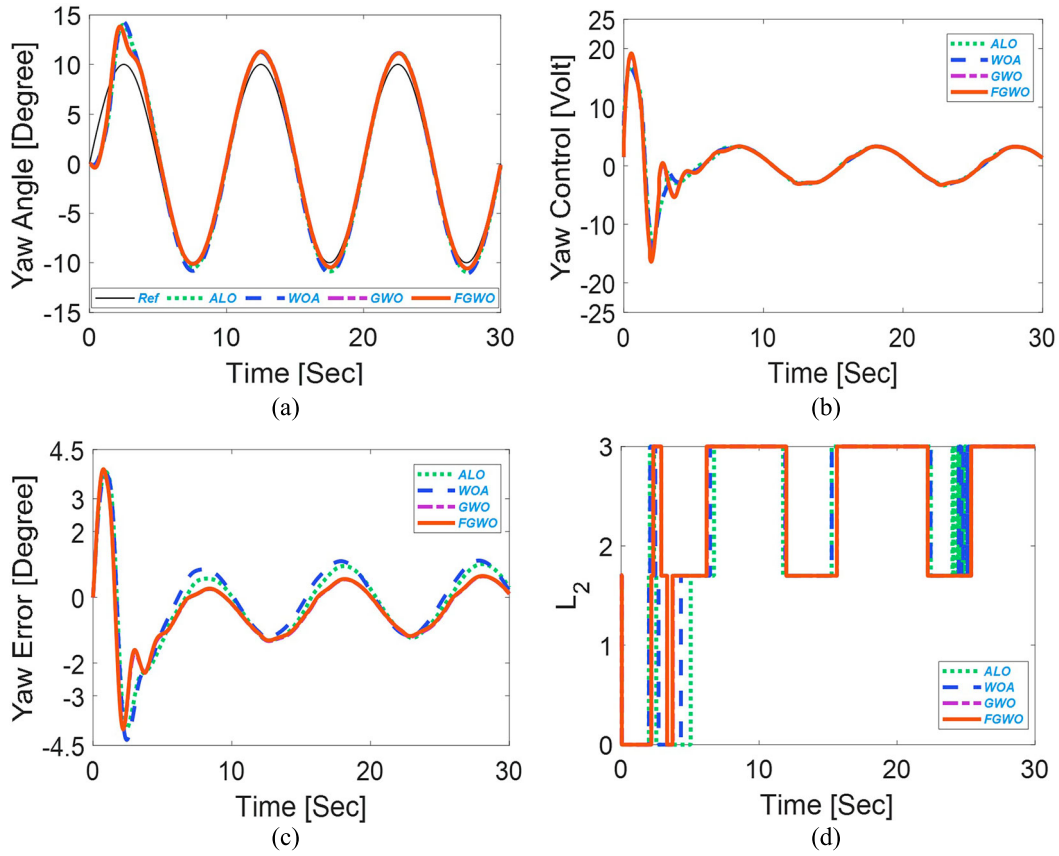


**Figure 18.** Simulation results of Dual FOPID RBFNN based on FGWO, GWO, WOA and ALO in trajectory tracking mode. (a) Yaw angle, (b) yaw control, (c) yaw error and (d) dual  $L_2$  parameter evolution.

**Table 8.** Error performance of Dual-RBFNN-FOPID based on ALO, WOA, GWO and FGWO ( $i = \theta$  or  $i = \psi$ ).

Angle	Dual-RBFNN-FOPID based on	ITAE	ISE	ISC	MAE	IAE
$(\theta) + (\psi)$ Regulation	ALO	1.2233e + 04	2.0015e + 04	4.7388e + 05	1.4515	7.2591e + 03
	WOA	9.7221e + 03	2.1159e + 04	4.8753e + 05	1.4086	7.0447e + 03
	GWO	8.9531e + 03	1.7128e + 04	<b>4.6092e + 05</b>	1.2150	6.0761e + 03
	FGWO	<b>8.5810e + 03</b>	<b>1.6911e + 04</b>	4.6371e + 05	<b>1.1933</b>	<b>5.9675e + 03</b>
	Rate of Improvement <sup>a</sup>	4.27%	1.26%	-0.6%	1.79%	1.79%
$(\theta) + (\psi)$ Trajectory tracking	ALO	1.9328e + 05	2.9726e + 04	<b>7.2581e + 05</b>	1.2282	1.8424e + 04
	WOA	1.9823e + 05	3.0682e + 04	7.3364e + 05	1.2430	1.8646e + 04
	GWO	1.6504e + 05	2.5056e + 04	7.3357e + 05	1.0898	1.6347e + 04
	FGWO	<b>1.6355e + 05</b>	<b>2.4947e + 04</b>	7.3981e + 05	<b>1.0825</b>	<b>1.6238e + 04</b>
	Rate of Improvement <sup>a</sup>	0.91%	0.44%	-1.89%	0.64%	0.66%

<sup>a</sup>Rate of Improvement obtained by DRF-FG compared with the second-best performance for each objective function.

is taken as a reference. In case of regulation mode, FGWO-based controllers improve ITAE, ISE, MAE and IAE by 4.3363%, 1.2832%, 1.8185%, and 1.8199% respectively. In trajectory tracking mode, these performance metrics are improved by 0.9110%, 0.4369%, 0.6744%, and 0.6713% for ITAE, ISE, MAE, and IAE, respectively. These results indicate that the proposed DRF-FG controller improves the control performance in terms of stabilization of the response. It is interesting to note that the control performance w.r.t. ISC index is observed to be the best in the case of GWO-based controller in the regulation mode and ALO-based controller in the trajectory tracking mode. From ISC point of view, the DRF-FG controller requires

more energy to achieve the best performance. The DRF-FG achieves the second-best performance w.r.t. ISC and the best performance w.r.t. ITAE, ISE, MAE and IAE and offers an average improvement rate of 1.702% in regulation mode and 0.152% in the trajectory tracking mode.

#### 6.4. Wind robustness test in trajectory tracking mode

The objective was to test the proposed controllers against external disturbances that imitate the wind effect. In addition to the disturbance analysis, a new desired trajectory given in (46) is considered here. The results are shown in

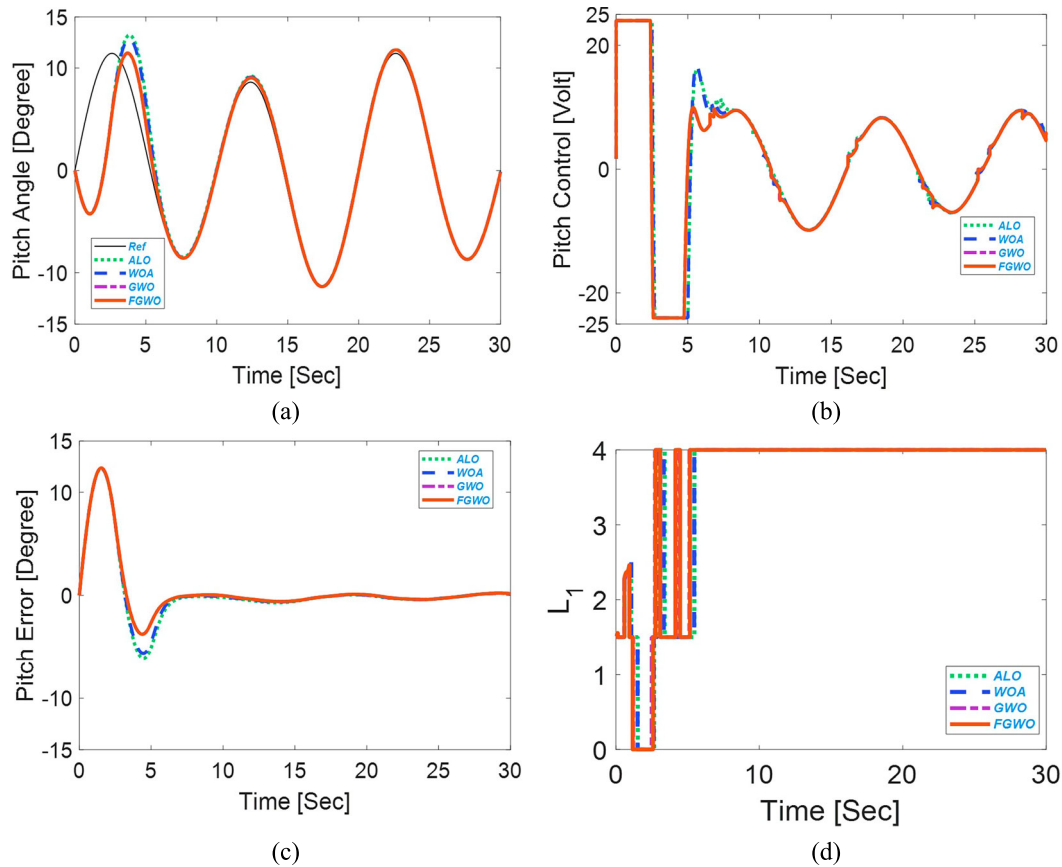


**Figure 19.** Simulation results of Dual FOPID RBFNN based on FGWO, GWO, WOA and ALO in disturbance test. (a) Pitch angle, (b) pitch control, (c) pitch error and (d) dual  $L_1$  parameter evolution.

Figures 19 and 20.

$$\left. \begin{aligned} \psi_{dist}(t) &= 10 \sin(0.1t) + 10 \sin(0.05t) \\ \varphi_{dist}(t) &= 10 \sin(0.1t) + 10 \sin(0.05t) \end{aligned} \right\} \quad (46)$$

The disturbance considered in this study is given in (47), which takes the same dynamic as the pitch and yaw references. However, the disturbance represents 10% of the desired yaw amplitude and 2% with the opposite sign of the desired pitch amplitude.

$$\left. \begin{aligned} \psi_{dist}(t) &= -0.2 \sin(0.1t) - 0.2 \sin(0.05t) \\ \varphi_{dist}(t) &= \sin(0.1t) + \sin(0.05t) \end{aligned} \right\} \quad (47)$$

From the simulation results of the trajectory tracking mode with and without disturbance, we can confirm that all the controllers demonstrated satisfactory performance. The optimized FOPID based on the proposed FGWO combined with RBFNN, referred to as DRF-FG, demonstrated superior results compared to those achieved based on ALO, WOA and standard GWO algorithms. It is observed that the overshoot is more noticeable in the case of DRF-FG for the pitch angle compared to the other controllers. However, in the steady state, the proposed controller offered the best performance with

zero steady-state error owing to the improvement contributed by RBFNN and dual part. For the yaw angle, DRF-FG and DRF-G provide practically the same response. It is also important to confirm that DRF-FG offers superior performance compared to the classical FOPID in all cases. From a control point of view, DRF-G, DRF-W and DRF-A consumed less energy. On the other hand, DRF-FG consumed more energy for both pitch and yaw angles, which improved the system responses.

## 7. Conclusion

This research presented a control-based metaheuristic optimization approach that carries novelty in two aspects. First, a new variant of GWO termed as FGWO is proposed. The combined ITAE and ISC, called IATESC, is used as a fitness function to verify the effectiveness of the proposed optimization algorithm. A comparative analysis of FGWO, GWO, WOA and ALO is performed. The algorithm is applied to a helicopter simulator to validate the proposed FGWO-FOPID. The simulation results show that the proposed approach is notably better than the classical GWO. The second novelty of this work lies in the proposed

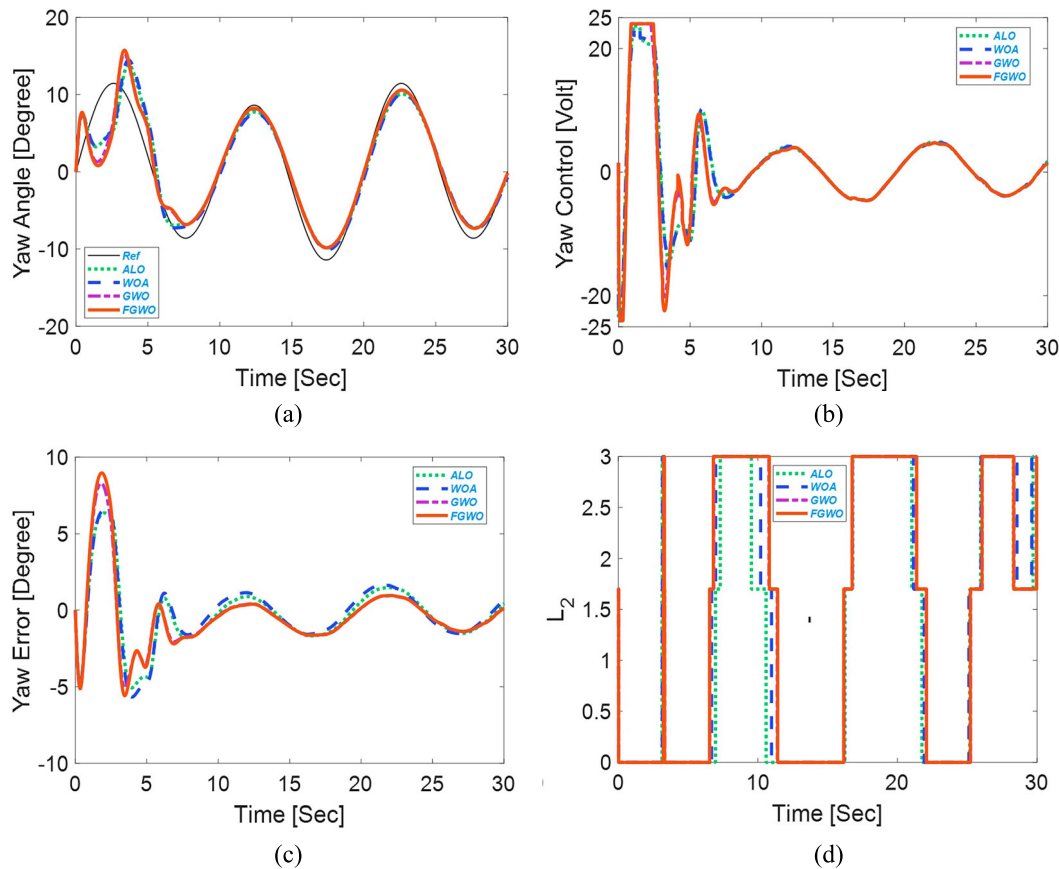


**Figure 20.** Simulation results of Dual FOPID RBFNN based on FGWO, GWO, WOA and ALO in disturbance test. (a) Yaw angle, (b) yaw control, (c) yaw error and (d) dual  $L_2$  parameter evolution.

Dual-RBFNN-FOPID-FGWO (DRF-FG) controller to handle the dynamics and coupling of the system. The application of FGWO-FOPID and RBFNN-FGWO-FOPID using a dual approach on a Quanser Aero helicopter simulator confirmed the superiority of the proposed controller over the Dual-RBFNN-FOPID based on GWO, WOA and ALO.

In the future, we plan to experimentally validate the proposed control approach by using a physical TITO helicopter system. Moreover, the modification of other terms of the GWO algorithm is envisaged. In addition, it could be interesting to consider a multi-objective criterion when testing the proposed FGWO algorithm.

### Acknowledgements

Amar Rezoug: Conceptualization, Methodology, Software, Formal analysis, Writing – original draft preparation; Jamshed Iqbal: Investigation, Validation, Supervision, Project administration, Writing – review and editing; Abdelkrim Nemra: Data curation, Study design, Visualization, Resources. All authors have read and approved the final version of the manuscript.

### Disclosure statement

No potential conflict of interest was reported by the author(s).

### Data availability statement

Data supporting the findings of this study are available from the first author (Amar Rezoug) upon a reasonable request.

### References

- Aero 2. (2024). 2 DOF PD control. <https://www.quanser.com/resource-type/academic-resources/>
- Chen, H., Ya, G., Li, J., Cui, H., & Yao, X. (2022). Predicting undrained shear strength of soil from cone penetration test data applying optimized RBF approaches. *Journal of Applied Science and Engineering*, 26(1), 121–130.
- Choubey, C., & Ohri, J. (2022). Tuning of LQR-PID controller to control parallel manipulator. *Neural Computing and Applications*, 34(4), 3283–3297. <https://doi.org/10.1007/s00521-021-06608-0>
- Choubey, C., & Ohri, J. (2023). GWO-based tuning of LQR-PID controller for a 3-DOF parallel manipulator. *IETE Journal of Research*, 69(7), 4378–4393. <https://doi.org/10.1080/03772063.2021.1958068>
- Dandago, K. K., Zhang, L., & Pan, W. (2024). *Fault detection and tolerant control for Aero2 2DOF two-rotor helicopter*. arXiv, preprint arXiv:2403.09008.
- Faisal, R. F., & Abdulwahhab, O. W. (2021). Design of an adaptive linear quadratic regulator for a twin rotor aerodynamic system. *Journal of Control, Automation and Electrical Systems*, 32(2), 404–415. <https://doi.org/10.1007/s40313-020-00682-w>

- Gopmandal, F., & Ghosh, A. (2022). LQR-based MIMO PID control of a 2-DOF helicopter system with uncertain cross-coupled gain. *IFAC-PapersOnLine*, 55(22), 183–188. <https://doi.org/10.1016/j.ifacol.2023.03.031>
- Guo, H., Chen, M., Jiang, Y., & Lungu, M. (2023). Distributed adaptive human-in-the-loop event-triggered formation control for QUAVs with quantized communication. *IEEE Transactions on Industrial Informatics*, 19(6), 7572–7582. <https://doi.org/10.1109/TII.2022.3211508>
- Haq, U. I., Khan, Q., Khan, S. A., Ullah, S., Akmelawati, R., Khan, M. A., & Iqbal, J. (2022). Neural network-based adaptive global sliding mode MPPT controller design for stand-alone photovoltaic systems. *PLoS ONE*, 17(1), e0260480.
- Haruna, A., Mohamed, Z., Efe, M. Ö., & Abdullahi, A. M. (2023). Switched step integral backstepping control for nonlinear motion systems with application to a laboratory helicopter. *ISA Transactions*, 141, 470–481. <https://doi.org/10.1016/j.isatra.2023.07.002>
- Haruna, A., Mohamed, Z., Efe, M. Ö., & Basri, M. A. M. (2020). Improved integral backstepping control of variable speed motion systems with application to a laboratory helicopter. *ISA Transactions*, 97, 1–13. <https://doi.org/10.1016/j.isatra.2019.07.016>
- Hoffman, D., Rehan, M., MacKunis, W., & Reyhanoglu, M. (2018). Quaternion-based robust trajectory tracking control of a quadrotor hover system. *International Journal of Control, Automation and Systems*, 16(6), 2575–2584. <https://doi.org/10.1007/s12555-018-0112-z>
- Huang, G., Cai, Y., Liu, J., & Qi, Y. (2021). A novel hybrid discrete grey wolf optimizer algorithm for multi-UAV path planning. *Journal of Intelligent & Robotic Systems*, 103(3), 49. <https://doi.org/10.1007/s10846-021-01490-3>
- Hussein, S. M., & Al-Araji, A. S. (2024). Development of path-finding controller design for hovercraft model via neural network technique and meta-heuristic algorithms. *International Journal of Intelligent Engineering and Systems*, 17(4), 576–597. <https://doi.org/10.22266/ijies2021.0831.44>
- Iqbal, J., Ullah, M. I., Khan, A. A., & Irfan, M. (2015). Towards sophisticated control of robotic manipulators: Experimental study on a pseudo-industrial arm. *Strojniški vestnik – Journal of Mechanical Engineering*, 61(7-8), 465–470. <https://doi.org/10.5545/sv-jme.2015.2511>
- Irfan, S., Zhao, L., Ullah, S., Javaid, U., & Iqbal, J. (2024). Differentiator and observer-based feedback linearized advanced nonlinear control strategies for an unmanned aerial vehicle system. *Drones*, 8(10), 527. <https://doi.org/10.3390/drones8100527>
- Izci, D., & Ekinci, S. (2023). Fractional order controller design via gazelle optimizer for efficient speed regulation of micromotors. *e-Prime – Advances in Electrical Engineering, Electronics and Energy*, 6, 100295. <https://doi.org/10.1016/j.prime.2023.100295>
- Izci, D., Köse, E., & Ekinci, S. (2023). Feedforward-compensated PI controller design for air–fuel ratio system control using enhanced weighted mean of vectors algorithm. *Arabian Journal for Science and Engineering*, 48(9), 12205–12217. <https://doi.org/10.1007/s13369-023-07724-w>
- Jarray, R., Al-Dhaifallah, M., Rezk, H., & Bouallague, S. (2022). Parallel cooperative coevolutionary grey wolf optimizer for path planning problem of unmanned aerial vehicles. *Sensors*, 22(5), 1826. <https://doi.org/10.3390/s22051826>
- Karakoyun, M., Ozkis, A., & Kodaz, H. (2020). A new algorithm based on grey wolf optimizer and shuffled frog leaping algorithm to solve the multi-objective optimization problems. *Applied Soft Computing*, 96, 106560. <https://doi.org/10.1016/j.asoc.2020.106560>
- Liu, Q., Li, D., Ge, S. S., Ji, R., Ouyang, Z., & Tee, K. P. (2021). Adaptive bias RBF neural network control for a robotic manipulator. *Neurocomputing*, 447, 213–223. <https://doi.org/10.1016/j.neucom.2021.03.033>
- Lopez-Sanchez, I., & Moreno-Valenzuela, J. (2023). PID control of quadrotor UAVs: A survey. *Annual Reviews in Control*, 56, 100900. <https://doi.org/10.1016/j.arcontrol.2023.100900>
- Luo, K. (2019). Enhanced grey wolf optimizer with a model for dynamically estimating the location of the prey. *Applied Soft Computing*, 77, 225–235. <https://doi.org/10.1016/j.asoc.2019.01.025>
- Lv, J. X., Yan, L. J., Chu, S. C., Cai, Z.-M., Pan, J.-S., He, X.-K., & Xue, J.-K. (2022). A new hybrid algorithm based on golden eagle optimizer and grey wolf optimizer for 3D path planning of multiple UAVs in power inspection. *Neural Computing and Applications*, 34(14), 11911–11936. <https://doi.org/10.1007/s00521-022-07080-0>
- Makhadmeh, S. N., Al-Betar, M. A., Doush, I. A., Awadallah, M. A., Kassaymeh, S., Mirjalili, S., & Zitar, R. A. (2024). Recent advances in Grey Wolf Optimizer, its versions and applications: Review. *IEEE Access*, 12, 22991–23028. <https://doi.org/10.1109/ACCESS.2023.3304889>
- Messaoui, A. Z., Mechali, O., Messaoui, A. A., Smaali, I. E., Demim, F., & Djilali, D. B. (2024). RBFNN-based optimized PID control for a 3-DOF helicopter system: Design and validation. In *2024 8th International Conference on Image and Signal Processing and their Applications (ISPA)* (pp. 1–5). IEEE.
- Mirjalili, S., & Lewis, A. (2016). The whale optimization algorithm. *Advances in Engineering Software*, 95, 51–67. <https://doi.org/10.1016/j.advengsoft.2016.01.008>
- Mirjalili, S., Mirjalili, S. M., & Lewis, A. (2014). Grey wolf optimizer. *Advances in Engineering Software*, 69, 46–61. <https://doi.org/10.1016/j.advengsoft.2013.12.007>
- Norsahperi, N. M. H., & Danapalasingam, K. A. (2020). Particle swarm-based and neuro-based FOPID controllers for a twin rotor system with improved tracking performance and energy reduction. *ISA Transactions*, 102, 230–244. <https://doi.org/10.1016/j.isatra.2020.03.001>
- Oliveira, J., Oliveira, P. M., Boaventura-Cunha, J., & Pinho, T. (2020). Evaluation of hunting-based optimizers for a quadrotor sliding mode flight controller. *Robotics*, 9(2), 22. <https://doi.org/10.3390/robotics9020022>
- Pathan, E., Khan, M. H., Aslam, M. K., Asad, M., Arshad, H., & Rabani, M. I. (2021). A multivariable twin-rotor system control design. *Engineering, Technology & Applied Science Research*, 11(1), 6626–6631. <https://doi.org/10.48084/etasr.3947>
- Qu, C., Gai, W., Zhong, M., & Zhang, J. (2020). A novel reinforcement learning based grey wolf optimizer algorithm for unmanned aerial vehicles (UAVs) path planning. *Applied Soft Computing*, 89, 106099. <https://doi.org/10.1016/j.asoc.2020.106099>
- Rezoug, A., Iqbal, J., & Tadjine, M. (2022). Extended grey wolf optimization-based adaptive fast nonsingular terminal sliding mode control of a robotic manipulator. *Proceedings of the Institution of Mechanical Engineers, Part I: Journal of Systems and Control Engineering*, 236(9), 1738–1754. <https://doi.org/10.1177/09596518221099768>
- Rezoug, A., Messah, A., Messaoud, W. A., Baizid, K., & Iqbal, J. (2024). Adaptive-optimal MIMO nonsingular terminal

- sliding mode control of twin-rotor helicopter system: Meta-heuristics and super-twisting based control approach. *Journal of the Brazilian Society of Mechanical Sciences and Engineering*, 46(3), 162. <https://doi.org/10.1007/s40430-024-04714-3>
- Shah, A. Q., Awais, M., Zafar, M., Ahmed, A., Mudassar, M., Muneer, M., Saif, M., Razzaq, A., Jang, S.-H., Kim, S., & Park, Y. (2023). A comparative study of linear control strategies on the aerodynamics twin rotor system. *Journal of Mechanical Science and Technology*, 37(8), 4301–4310. <https://doi.org/10.1007/s12206-023-0746-5>
- Shalaby, R., El-Hossainy, M., Abo-Zalam, B., & Mahmoud, T. A. (2023). Optimal fractional-order PID controller based on fractional-order actor-critic algorithm. *Neural Computing and Applications*, 35(3), 2347–2380. <https://doi.org/10.1007/s00521-022-07710-7>
- Shauqee, M. N., Rajendran, P., & Suhadis, N. M. (2021). Proportional double derivative linear quadratic regulator controller using improvised grey wolf optimization technique to control quadcopter. *Applied Sciences*, 11(6), 2699. <https://doi.org/10.3390/app11062699>
- Singh, V. K., Kamal, S., & Ghosh, S. (2023). Prescribed-time constrained feedback control for an uncertain twin rotor helicopter. *Aerospace Science and Technology*, 140, 108483. <https://doi.org/10.1016/j.ast.2023.108483>
- Sreedhar, R., Karunanithi, K., Ramesh, S., Raja, S. P., & Pasham, N. K. (2024). Optimizing grid connected photovoltaic systems using elementary LUO converter and GWO-RBFNN based MPPT. *Electrical Engineering*, <https://doi.org/10.1007/s00202-024-02637-9>
- Sun, Y., & Miao, J. (2023, November). Research on unmanned aerial vehicle flight attitude control method based on sparrow search algorithm and PID optimization. In *UAVM '23: Proceedings of the 2023 Workshop on UAVs in Multimedia: Capturing the World from a New Perspective* (pp. 73–77). <https://doi.org/10.1145/3607834.3616565>
- Tripathi, S., Shrivastava, A., & Jana, K. C. (2020). Self-tuning fuzzy controller for sun-tracker system using gray wolf optimization (GWO) technique. *ISA Transactions*, 101, 50–59. <https://doi.org/10.1016/j.isatra.2020.01.012>
- Tutsoy, O., Hendoustani, D., Ahmadi, K., Nabavi, Y., & Iqbal, J. (2024). Minimum distance and minimum time optimal path planning with bioinspired machine learning algorithms for impaired unmanned air vehicles. *IEEE Transactions on Intelligent Transportation Systems*, 25(8), 9069–9077. <https://doi.org/10.1109/TITS.2024.3367769>
- Veerasamy, V., Wahab, N. I. A., Ramachandran, R., Othman, M. L., Hizam, H., Kumar, J. S., & Irudayaraj, A. X. R. (2022). Design of single- and multi-loop self-adaptive PID controller using heuristic based recurrent neural network for ALFC of hybrid power system. *Expert Systems with Applications*, 192, 116402. <https://doi.org/10.1016/j.eswa.2021.116402>
- Wang, G., Feng, D., & Tang, W. (2022). Electrical impedance tomography based on grey wolf optimized radial basis function neural network. *Micromachines*, 13(7), 1120. <https://doi.org/10.3390/mi13071120>
- Wang, R., Zhou, Z., & Qu, G. (2018, October). Fuzzy neural network PID control based on RBF neural network for variable configuration spacecraft. In *2018 IEEE 3rd Advanced Information Technology, Electronic and Automation Control Conference (IAEAC)* (pp. 1203–1207). IEEE.
- Wu, J., Fang, L., Dong, G., & Lin, M. (2023). State of health estimation of lithium-ion battery with improved radial basis function neural network. *Energy*, 262, 125380. <https://doi.org/10.1016/j.energy.2022.125380>
- Yang, Q., Wang, H., Yang, C., Wang, Y., Hu, D., Wang, B., & Duan, B. (2024). Research on surrogate models and optimization algorithms of compressor characteristic based on digital twins. *Journal of Engineering Research*. <https://doi.org/10.1016/j.jer.2024.01.025>
- Yingxun, W., Zhang, T., Zhihao, C., Jiang, Z., & Kun, W. (2020). Multi-UAV coordination control by chaotic grey wolf optimization based distributed MPC with event-triggered strategy. *Chinese Journal of Aeronautics*, 33(11), 2877–2897. <https://doi.org/10.1016/j.cja.2020.04.028>
- Zatout, M. S., Rezoug, A., Baizid, K., & Iqbal, J. (2022). Optimization of fuzzy logic quadrotor attitude controller – Particle swarm, cuckoo search and BAT algorithms. *International Journal of Systems Science*, 53(4), 883–908. <https://doi.org/10.1080/00207721.2021.1978012>
- Żegleń-Włodarczyk, J. (2023). FOPID and PID-comparison of control quality and execution time on the example of two rotor aerodynamical system. In R. Szweczyk, C. Zieliński, M. Kaliczńska, & V. Bučinskas (Eds.), *Conference on Automation* (pp. 29–38). Springer Nature Switzerland. [https://doi.org/10.1007/978-3-031-25844-2\\_3](https://doi.org/10.1007/978-3-031-25844-2_3)
- Zeng, X., Wang, W., & Wang, H. (2022). Adaptive PI and RBFNN PID current decoupling controller for permanent magnet synchronous motor drives: Hardware-validated results. *Energies*, 15(17), 6353. <https://doi.org/10.3390/en15176353>
- Zhang, R., Li, S., Ding, Y., Qin, X., & Xia, Q. (2022). UAV path planning algorithm based on improved Harris Hawks optimization. *Sensors*, 22(14), 5232. <https://doi.org/10.3390/s22145232>
- Zhang, X., & Ming, Z. (2021). Par4 parallel robot trajectory tracking control based on DMR-GWO2 and fuzzy predictive. *International Journal of Computational Intelligence Systems*, 14(1), 1597–1606. <https://doi.org/10.2991/ijcis.d.210514.001>
- Zhu, X., & Li, D. (2021). Robust fault estimation for a 3-DOF helicopter considering actuator saturation. *Mechanical Systems and Signal Processing*, 155, 107624. <https://doi.org/10.1016/j.ymssp.2021.107624>
- Zijie, N., Peng, Z., Cui, Y., & Jun, Z. (2022). PID control of an omnidirectional mobile platform based on an RBF neural network controller. *Industrial Robot: The International Journal of Robotics Research and Application*, 49(1), 65–75. <https://doi.org/10.1108/IR-01-2021-0015>

## Appendix

**Table A1.** RBFNN parameters.

		$N^*$	$W$	$C$	$b$
Pitch RBFNN-parameters	$P$	9	(0.005, 0.002, 0.005, 0.001, 0.2, 0.58, 0.4, 0.007, 0.008, 0.005)	(0.9, 0.5, 0.8, 0.7, 0.2, 0.5, 0.47, 0.5, 0.9, 0.5)	(0.02, 0.06, 0.09, 0.04, 0.007, 0.1, 0.5, 0.5, 0.7, 0.8)
	$I$	4	(0.1, 0.2, 0.3, 0.4)	(0.1, 0.2, 0.5, 0.4)	(0.1, 0.2, 0.1, 0.2)
	$D$	7	(0.000001, 0.000002, 0.000003, 0.0000047, 0.000001, 0.000006, 0.000002)	(0.01, 0.034, 0.02, 0.02, 0.03, 0.06, 0.2)	(0.002, 0.0019, 0.002, 0.005, 0.003, 0.006, 0.002)
Yaw RBFNN parameters	$P$	10	(0.00012, 0.0005, 0.0004, 0.00021, 0.0005, 0.006, 0.0005, 0.004, 0.0078, 0.005)	(0.1, 0.01, 0.15, 0.015, 0.3, 0.6, 0.5, 0.47, 0.98, 0.58)	(0.2, 0.2, 0.3, 0.3, 0.6, 0.14, 0.58, 0.57, 0.9, 0.7)
	$I$	10	(0.00012, 0.0005, 0.0004, 0.00021, 0.0005, 0.006, 0.0005, 0.004, 0.0078, 0.005)	(0.1, 0.01, 0.15, 0.015, 0.3, 0.6, 0.5, 0.47, 0.98, 0.58)	(0.2, 0.2, 0.3, 0.3, 0.6, 0.14, 0.58, 0.57, 0.9, 0.7)
	$D$	7	(0.00005, 0.000021, 0.000003, 0.000008, 0.000002, 0.000005, 0.00003)	(0.01, 0.02, 0.04, 0.02, 0.01, 0.05, 0.2)	(0.0031, 0.0079, 0.0052, 0.0088, 0.0063, 0.005, 0.003)

Note:  $N^*$  number of neurons in handle layer.